



Article

Discovery and Optimization of Triazine Nitrile Inhibitors of Toxoplasma gondii Cathepsin L for the Potential Treatment of Chronic Toxoplasmosis in the CNS

Jeffery D. Zwicker, David Smith, Alfredo J. Guerra, Jacob R Hitchens, Nicole Haug, Steve Vander Roest, Pil Lee, Bo Wen, Duxin Sun, Lu Wang, Richard Keep, Jianming Xiang, Vern B. Carruthers, and Scott D Larsen

ACS Chem. Neurosci., **Just Accepted Manuscript** • DOI: 10.1021/acchemneuro.9b00674 • Publication Date (Web): 06 Feb 2020

Downloaded from pubs.acs.org on February 6, 2020

Just Accepted

“Just Accepted” manuscripts have been peer-reviewed and accepted for publication. They are posted online prior to technical editing, formatting for publication and author proofing. The American Chemical Society provides “Just Accepted” as a service to the research community to expedite the dissemination of scientific material as soon as possible after acceptance. “Just Accepted” manuscripts appear in full in PDF format accompanied by an HTML abstract. “Just Accepted” manuscripts have been fully peer reviewed, but should not be considered the official version of record. They are citable by the Digital Object Identifier (DOI®). “Just Accepted” is an optional service offered to authors. Therefore, the “Just Accepted” Web site may not include all articles that will be published in the journal. After a manuscript is technically edited and formatted, it will be removed from the “Just Accepted” Web site and published as an ASAP article. Note that technical editing may introduce minor changes to the manuscript text and/or graphics which could affect content, and all legal disclaimers and ethical guidelines that apply to the journal pertain. ACS cannot be held responsible for errors or consequences arising from the use of information contained in these “Just Accepted” manuscripts.

1
2
3
4
5
6
7
8
9
10
11
12

Discovery and Optimization of Triazine Nitrile Inhibitors of *Toxoplasma gondii* Cathepsin L for the Potential Treatment of Chronic Toxoplasmosis in the CNS

13
14
15
16
17
18
19
20

Jeffery D. Zwicker^{†,‡}, David Smith[‡], Alfredo J. Guerra[‡], Jacob R. Hitchens^{†,‡}, Nicole Haug[‡], Steve Vander
Roest[#], Pil Lee^{†,‡}, Bo Wen[§], Duxin Sun[§], Lu Wang[§], Richard F. Keep⁺, Jianming Xiang⁺, Vern B.
Carruthers[‡], and Scott D. Larsen^{*†,‡}

21
22
23
24

[†]Vahlteich Medicinal Chemistry Core, College of Pharmacy, University of Michigan, Ann Arbor,
Michigan 48109, United States

25
26
27

[‡]Department of Medicinal Chemistry, University of Michigan, Ann Arbor, Michigan 48109, United States

28
29
30
31

[‡]Department of Microbiology and Immunology, University of Michigan, Ann Arbor, Michigan 48109,
United States

32
33

[#]Center for Chemical Genomics, Life Sciences Institute, Ann Arbor, MI 48109, United States

34
35
36
37

[§]Pharmacokinetics Core, Department of Pharmaceutical Sciences, University of Michigan, Ann Arbor,
Michigan 48109, United States

38
39
40

⁺Department of Neurosurgery, University of Michigan, Ann Arbor, Michigan 48109, United States

41
42
43
44
45
46

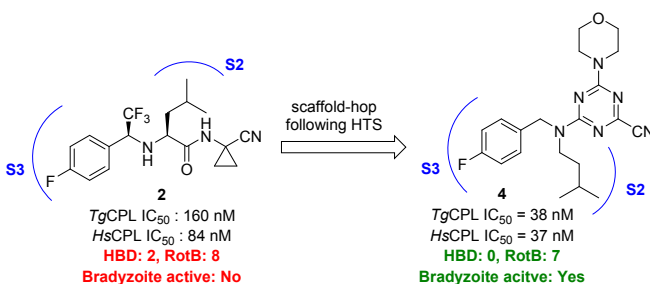
*Corresponding author. E-mail address: sdlarsen@med.umich.edu

47
48
49
50
51
52

KEYWORDS: *Toxoplasma gondii*, antiparasitics, toxoplasmosis, cathepsin L, triazine nitrile, protease,
infectious disease, antiprotazoal agents, blood-brain barrier, central nervous system

Abstract: With roughly 2 billion people infected, the neurotropic protozoan *Toxoplasma gondii* remains one of the most pervasive and infectious parasites. *Toxoplasma* infection is the 2nd leading cause of death due to foodborne illness in the US, causes severe disease in immunocompromised patients, and is correlated with several cognitive and neurological disorders. Currently, no therapies exist capable of eliminating the persistent infection in the central nervous system (CNS). In this study we report the identification of triazine nitrile inhibitors of *Toxoplasma* cathepsin L (*TgCPL*) from a high throughput screen, and their subsequent optimization. Through rational design, we improved inhibitor potency to as low as 5 nM, identified pharmacophore features that can be exploited for isoform selectivity (up to 7-fold for *TgCPL* versus human isoform), and improved metabolic stability ($t_{1/2} > 60$ min in mouse liver microsomes) guided by a metabolite ID study. We demonstrated this class of compounds is capable of crossing the blood-brain barrier in mice (1:1 Brain:Plasma at 2 hr). Importantly, we also show for the first time that treatment of *T. gondii* bradyzoite cysts in vitro with triazine nitrile inhibitors reduces parasite viability with efficacy equivalent to a *TgCPL* genetic knockout.

Graphical Abstract:



INTRODUCTION

Estimates suggest over 30% of the global human population is currently infected with *Toxoplasma gondii*, with approximately 60 million infected in the United States alone.¹⁻³ Capable of infecting nearly all warm-blooded mammals, this single-celled apicomplexan is the second leading cause of death due to foodborne illness in the US.⁴ As a member of the phylum Apicomplexa, *Toxoplasma gondii* exhibits a complex infection cycle in humans.⁵ Through consumption of contaminated food, or direct exposure to cat fecal matter, the parasite enters an initial tachyzoite infection stage, in which the parasite undergoes rapid asexual replication and disseminates throughout the host tissues, including the central nervous system (CNS).⁶ Upon activation of the host immune response, *T. gondii* transforms into its chronic bradyzoite phase, in which the parasite exists as lifelong tissue cysts within the muscle and CNS. If the host maintains a healthy immune system, this chronic infection generally presents few symptoms, although recently there is a growing body of evidence suggesting that this chronic stage infection may significantly contribute to a wide array of neuropsychiatric symptoms including schizophrenia, bipolar disorder, obsessive compulsive disorder, and various other mood alterations.⁷⁻¹⁰

A more obvious impact on human health from this parasite is revealed when the host immune system is compromised. The unchecked parasite cysts reactivate into the acute tachyzoite form, causing tissue inflammation and more serious complications such as: encephalitis, blindness, and death.¹¹ Treatment options for toxoplasmosis reactivation are generally pyrimethamine in combination with sulfadiazine, or clindamycin.¹² However, these options are prone to adverse side effects and only act upon the parasite in the peripheral system. Currently, no approved treatment options exist to clear the latent and chronic *Toxoplasma* infection in the CNS, therefore it is critical to develop new and alternative treatment strategies. A recent review by Deng et al¹³ summarizes current approaches to targeting enzymes critical to the life cycle of the parasite, including calcium-dependent protein kinase 1 (TgCDPK1), thymidylate synthase-dihydrofolate reductase, enoyl-acyl carrier protein reductase, and cathepsin L. TgCDPK1 inhibitors in particular have shown promise for treating the chronic form of *T. gondii*.¹⁴

1
2
3
4
5
6
7
8
9
10
11
12
13
14
15
16
17
18
19
20
21
22
23
24
25
26
27
28
29
30
31
32
33
34
35
36
37
38
39
40
41
42
43
44
45
46
47
48
49
50
51
52
53
54
55
56
57
58
59
60

Cathepsins L and B are the major cysteine proteases found in protozoans, and are emerging as viable targets for anti-parasitic agents due to their essential roles in parasite survival.¹⁵⁻¹⁷ For example, Rhodesain (*T. brucei*), cruzain (*T. cruzi*), and falcipain (*P. falciparum*) express cathepsin L-like proteases that have gained a considerable amount of attention for the potential treatment of African sleeping sickness, Chagas disease, and malaria respectively.¹⁸ *Toxoplasma gondii* expresses five members of the C1 family of cysteine proteases, including *TgCPL*, *TgCPB*, and *TgCPC1-3*.¹⁹⁻²² *TgCPL* is localized in the plant like-vacuole (PLV) vacuolar compartment (VAC, used hereafter), and is also responsible for the maturation and activation of *TgCPB*.^{20, 23} Although inhibition or disruption of *TgCPL* in the parasite has been shown to moderately impede parasite invasion and growth in the tachyzoite stage of infection, *TgCPL* is not critical to the acute stage.^{21, 23} Interestingly, parasites in the cystic bradyzoite stage express heightened levels of *TgCPL* and *TgCPB*, suggesting proteolysis in the VAC plays an important role in the chronic infection.²⁴ Accordingly, bradyzoites deficient in *TgCPL* die after forming cysts in both culture and in the neuronal cells of infected mice. Upon restoration of catalytically active *TgCPL*, bradyzoite viability is re-established. In contrast, expression of a catalytically inactive *TgCPL* fails to restore cyst viability. Taken together, these strongly implicate *TgCPL* as a viable target for the treatment of this chronic stage infection. The parasite dependence on *TgCPL* has been further validated in vitro, as well as through the treatment of cysts with the covalent, irreversible cathepsin inhibitor LHVS (**1**, **Figure 1**).²⁵ This disruption of the proteolytic activity in the lysosomal VAC ultimately results in parasite death.²⁶ However, LHVS is not a viable pharmaceutical lead as it failed to reduce neural cysts in infected mice, due to its poor drug-like properties (e.g., fails to cross the blood-brain barrier).²⁷

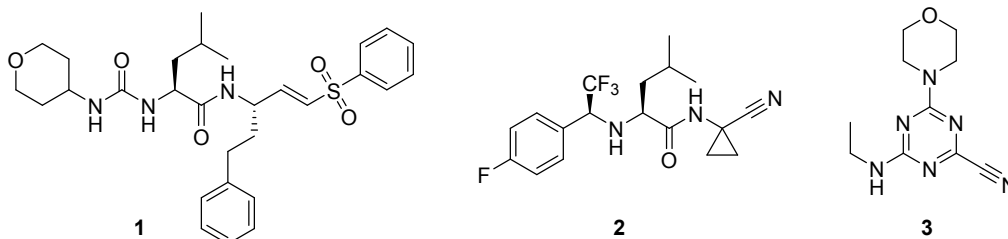
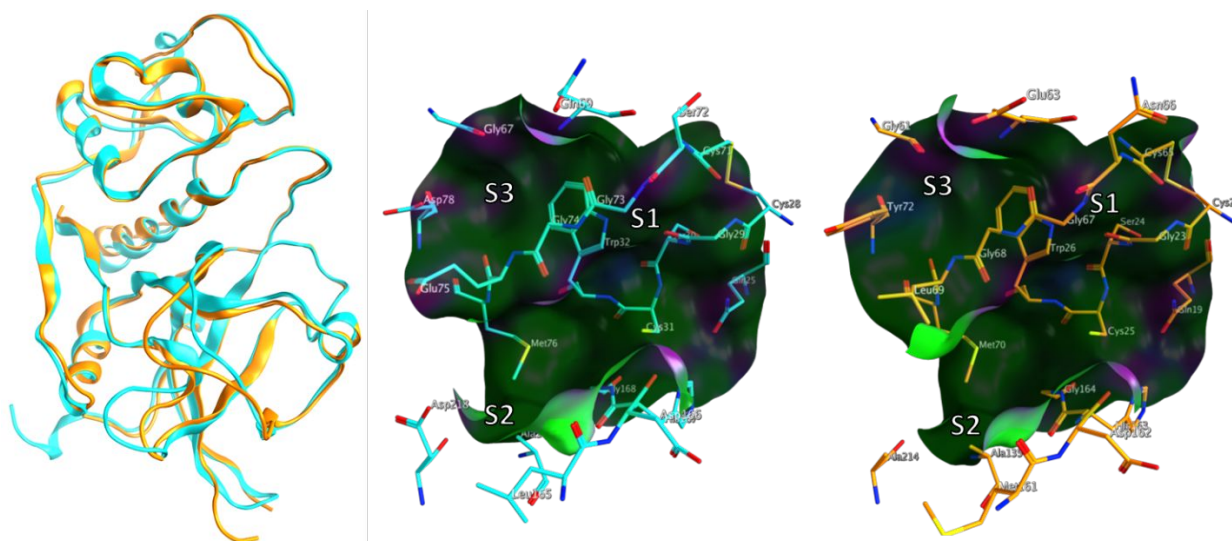


Figure 1. Inhibitors of *Toxoplasma gondii* cathepsin L

1
2
3
4
5
6 Recently, we reported the first lead optimization study for the inhibition of *TgCPL* with a series
7 of dipeptide nitriles.²⁸ While we were able to gain insight into the pharmacophore necessary for *TgCPL*
8 inhibition and significantly improve the potency and selectivity over human isoforms, we were unable to
9 carry forward the dipeptide series due to the inadequate pharmacokinetic (PK) properties of optimized
10 lead **2**. Despite being potent in vitro and demonstrably CNS penetrant, the drug was rapidly cleared in
11 vivo. While the dipeptide-nitriles are synthetically convenient for investigating SAR in the cathepsin
12 pockets, they have less than desirable physiochemical properties for gaining robust blood-brain barrier
13 (BBB) permeability, such as several rotational bonds, extensive hydrogen bonding, and high topological
14 polar surface area (TPSA).²⁹ We thus began searching for alternative scaffolds that might exhibit better
15 physiochemical properties to improve upon the in vivo PK, while maintaining the pharmacophoric
16 elements necessary for potent *TgCPL* inhibition.
17
18
19
20
21
22
23
24
25
26
27
28
29
30

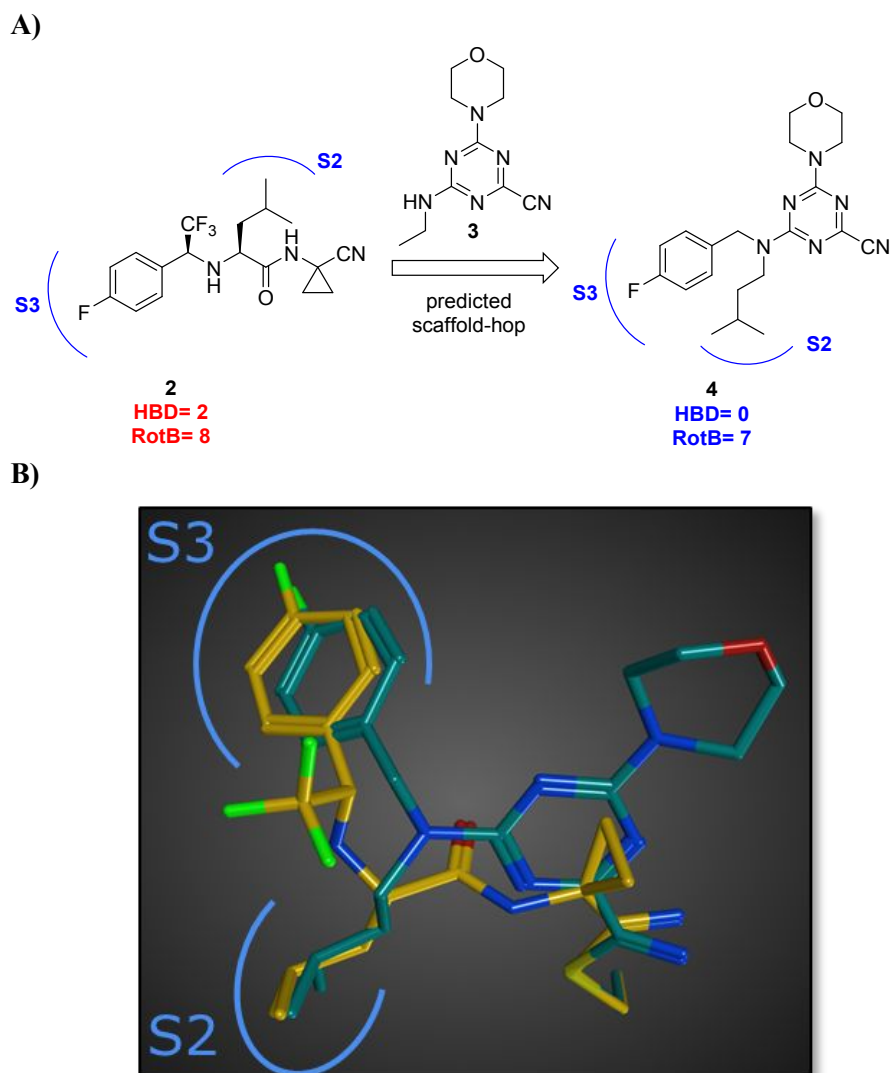


31
32
33
34
35
36
37
38
39
40
41
42
43
44
45
46
47 **Figure 2:** Structural overlay and active sites of apo *TgCPL* (Cyan; PDB-3F75) and apo *HsCPL* (Orange
48 PDB-5MAJ)
49
50
51
52
53
54
55
56
57
58
59
60

1
2
3 A high throughput screen for *TgCPL* inhibitors was conducted at the Center for Chemical
4 Genomics at the University of Michigan on over 150,000 small molecules. From this we identified
5 several inhibitor classes that demonstrated promising inhibitory activity against *TgCPL*, reasonable
6 synthetic approachability, and physiochemical profiles optimal for use as a lead scaffold in a CNS
7 targeted campaign. To minimize potential PK and off-target toxicity issues in later development, we
8 chose to exclude compounds that were peptidic in structure, or irreversibly covalent. After our triage
9 process had identified several potential lead molecules, we searched the literature to determine if any of
10 these chemotypes had any previously demonstrated activity against cysteine proteases. An extensive
11 amount of study has been done on inhibitors of human cathepsin L (*HsCPL*).³⁰ Since *Toxoplasma gondii*
12 cathepsin L shares high homology with *HsCPL*, we considered chemotypes with precedent for inhibiting
13 *HsCPL* as good potential leads. The overall sequence similarity between the two is about 50 %. However,
14 for residues within 4.5 Å of the triazine, the similarity is about 72 %. Only 5 out of 18 residues in the
15 binding site are different in the two structures (**Figure 2**). Among the several potential lead molecules
16 discovered in our screen, we selected a modestly active triazine nitrile **3** (*TgCPL* IC₅₀ = 2.5 μM, *HsCPL*
17 IC₅₀ = 2.3 μM) as a lead candidate (**Figure 1**), given its fragment-like size and solid literature precedent
18 as a cathepsin inhibitor class. Several recent publications have reported triazine nitrile-based inhibitors of
19 human cathepsins, and additionally demonstrated potent inhibition of rhodesain and falcipain.³¹⁻³³ The
20 activity reported against these analogous cysteine proteases from the related apicomplexan parasites *P.*
21 *falciparum* and *T. brucei* further supports the potential of this chemotype as an antiparasitic agent.
22 Additional triazine nitriles, pyrazolopyrimidine nitriles, and related heterocyclic-nitrile motifs have also
23 been reported as inhibitors of cysteine proteases.³⁴⁻³⁷

24
25
26
27
28
29
30
31
32
33
34
35
36
37
38
39
40
41
42
43
44
45
46
47
48
49
50 Although these recent studies have established the potential of this chemotype as a clinically relevant
51 antiparasitic agent, *Toxoplasma gondii*, as well as other protozoan parasites such as *T. brucei*, establish a
52 chronic infection in the CNS. Compounds intended for CNS targets have a somewhat constrained
53 physiochemical profile as compared to peripheral drugs. Key among these are the minimization of both
54
55
56
57
58
59
60

1
2
3 the number of hydrogen bond donors and rotatable bonds, which can increase the rate of passive BBB
4 penetration. Additionally, CNS drugs exhibit relatively low MW (<450), high lipophilicity (logP 2-5), and
5 exclusion of acidic moieties. The triazinyl-nitrile scaffold was particularly promising in that it could
6 readily incorporate the structural motifs necessary for binding in the S2 and S3 pockets of *TgCPL* (**Figure**
7 **2**), which we elucidated in our previous dipeptide work. This scaffold also has a potentially improved
8 pharmacokinetic profile and CNS permeability by reducing the rotational degrees of freedom, eliminating
9 a hydrolyzable amide and removing two hydrogen bond donors (HBD). Molecular docking and energy
10 minimization of the dipeptide nitrile (**2**) and proposed triazine nitrile (**4**) in the active site of *TgCPL*
11 showed good structural agreement into the pharmacophore of *TgCPL* inhibition (**Figure 3**). Altogether
12 this encouraged us to attempt a scaffold-hop from the optimized dipeptide to a triazine nitrile. In this
13 paper we report our success at this transformation, and our initial SAR work at enhancing selectivity for
14 the parasite enzyme vs human cathepsin L. Furthermore, we demonstrate for the first time the ability of
15 this class of compounds to inhibit bradyzoite viability in vitro and to penetrate into the brain in vivo, two
16 key milestones for developing an effective therapeutic for the chronic stage of *T. gondii*.
17
18
19
20
21
22
23
24
25
26
27
28
29
30
31
32
33
34
35
36
37
38
39
40
41
42
43
44
45
46
47
48
49
50
51
52
53
54
55
56
57
58
59
60



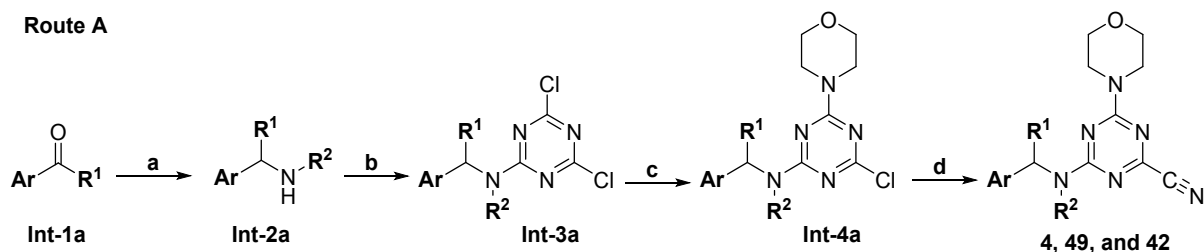
40
41
42
43
44
45
46
47
48
49
50
51
52
53
54
55
56
57
58
59
60

Figure 3. Predicted scaffold hop from optimized dipeptide nitrile to a triazine nitrile. **A)** Predicted projection of common vectors into the S2 and S3 sites of TgCPL based on computational docking of the dipeptide scaffold **2** and a corresponding triazine nitrile scaffold **4** into the crystal structure of TgCPL derived from PDB: 3F75. **B)** Molecular overlay of dipeptide nitrile (**2**, yellow) and triazine nitrile (**4**, teal) demonstrating good structural alignment.; HBD= Hydrogen bond donor; Rot B= rotatable bonds;

RESULTS AND DISCUSSION

Synthesis of TgCPL inhibitors

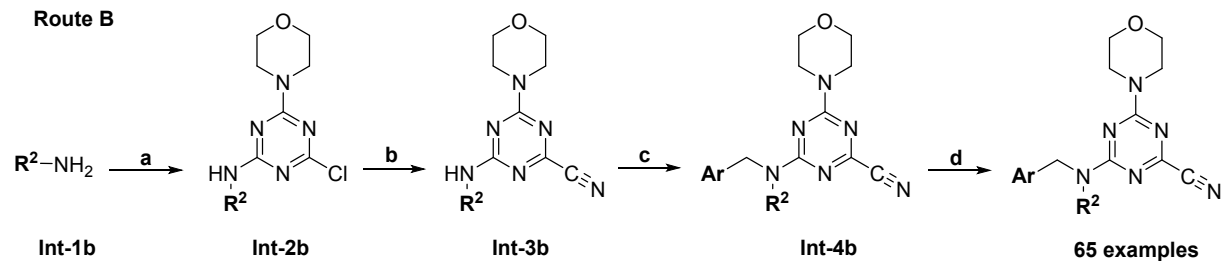
Scheme 1. General synthesis of triazine nitrile inhibitors



Reagents and conditions: a) R^2NH_2 , NaBH_4 , DCM, rt, or Titanium (IV) isopropoxide, $\text{Na(OAc)}_3\text{BH}$, DCM, 0°C -rt, O/N; b) cyanuric chloride, DIPEA, DCM, -10°C , 1-2 hr; c) morpholine, DIPEA, DCM, 0°C -rt, 4 hr; d) KCN, DMSO: H_2O (9:1), 80°C , O/N.

Under anhydrous conditions, the desired aryl aldehyde or acetophenone **Int-1a** was condensed with the desired alkylamine overnight, at which point the formed imine was reduced with sodium borohydride or sodium triacetoxyborohydride (**Scheme 1**). Next, the reaction between the secondary amine **Int-2a** and cyanuric chloride provided intermediates **Int-3a**. Subsequent $\text{S}_{\text{N}}\text{Ar}$ with morpholine afforded intermediates **Int-4a**. In the case of **50**, oxetanamine was used as the P1 solubilizing group in place of morpholine. Finally, cyanation of the scaffold with potassium cyanide in DMSO provided the desired final compounds.

Scheme 2. Alternative general synthesis of triazine nitrile inhibitors



Reagents and conditions: a) i. Cyanuric chloride, DIPEA, DCM, -10°C , 1-2 hr; ii. Morpholine, DIPEA, DCM, 0°C -rt, 4 hr; b) KCN, DMSO: H_2O (9:1), 80°C , O/N; c) NaH, DMF, 0°C 30 min, then ArCH_2X when $\text{X}=\text{Br}$, Cl, Ts, or Ms; d) TFA:DCM (1:2), rt, 0.5-1 hr.

1
2
3 To expedite rapid production of diverse analogs, a synthetic strategy analogous to that reported
4 by Giroud et. al. for the synthesis of triazine-nitrile *HsCPL* inhibitors was employed (**Scheme 2**).³¹ First,
5 cyanuric chloride underwent S_NAr reactions with the desired benzyl or alkyl amines **Int-1b** to set the
6 various S2 and S3 vectors for intermediates **Int-2b**. A second S_NAr step was employed to install a
7 morpholine as a P1 solubilizing group. Cyanation of the intermediate was performed with potassium
8 cyanide in DMSO, to afford **Int-3b**. Subsequently, the anion of intermediates **Int-3b** was generated using
9 sodium hydride, and the desired alkyl/benzyl halide was added to provide analogs **Int-4b**. In the case of
10 analogs bearing a Boc-protected amine side chain, TFA:DCM deprotection was employed to provide the
11 desired final compounds.
12
13
14
15
16
17
18
19
20
21
22
23
24

25 **Docking of the triazine scaffold into *TgCPL* and *HsCPL*:** The IC₅₀ for the triazine nitrile we
26 identified in our HTS (**3**) was benchmarked at 3.5 μM and 2.3 μM against *TgCPL* and *HsCPL*,
27 respectively (**Table 1**). Considering this lead bears an ethyl as the only potential P2/3 vector, it left
28 obvious room for improvement. As previously discussed (**Figure 3**), we elected to first synthesize the
29 triazine nitrile **4** analogous to an optimum dipeptide nitrile from our previous work. **Figure 4** presents a
30 comparison of models of **4** docked into the active sites of *TgCPL* and *HsCPL*. The triazine nitrile replaces
31 the P1-P2 amide bond and retains the reversibly covalent nitrile interaction with the active site cysteine.
32 In the P2 position, we previously found that leucine is the optimal dipeptide amino acid, so in the
33 respective position on the triazine, which we hypothesized would project into P2, we placed an isoamyl
34 amine to achieve the same length into the pocket. In P3, our most active compound previously bore a 4-
35 fluorobenzyl, and therefore we placed the same motif in the hypothetical P3 position for the triazine
36 nitrile scaffold. An additional feature found both in our HTS lead and known literature analogs was the P1
37 morpholine. While the S1 pocket in *TgCPL* is absent, the morpholine in the P1 position projects into
38 solvent and has been shown to improve the solubility of this chemotype (**Figure 4**).
39
40
41
42
43
44
45
46
47
48
49
50
51
52
53
54
55
56
57
58
59
60

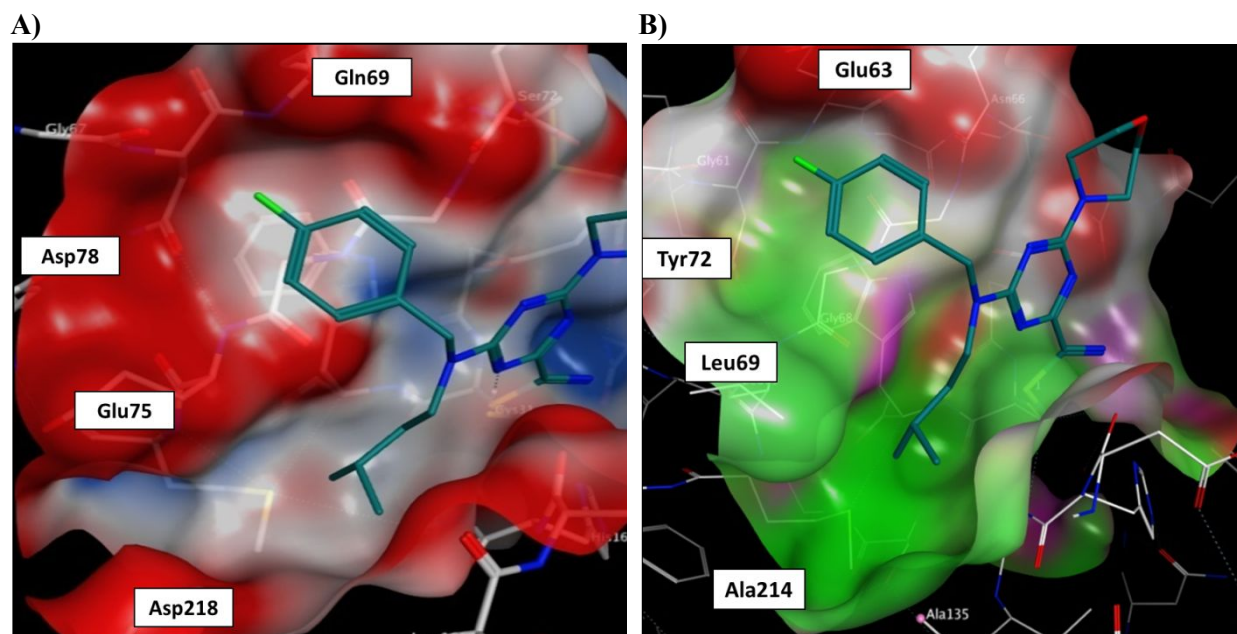


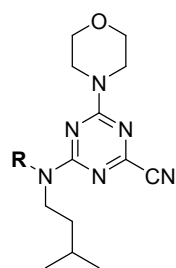
Figure 4. Comparison of *TgCPL* and *HsCPL* binding sites. **A)** Covalent docking of **4** into *TgCPL* active site and electrostatic surface mapping. Red= polar negative, White = neutral, Blue= polar positive. (Derived from PDB: 3F75); **B)** Covalent docking of **4** into the active site of *HsCPL* (PDB: 5MAJ). Pocket view; Red= polar negative, White= neutral, Green= lipophilic

The installment of these two pendants in our first triazine analog **4** indeed provided over a 100-fold improvement in potency over the HTS lead **3**, affording an IC_{50} of 34 nM and 32 nM for *TgCPL* and *HsCPL*, respectively (**Table 1**). These results supported our docking model, and validated our hypothesis that we could successfully scaffold-hop from the dipeptides to the triazine, suggesting that much of our dipeptide SAR should translate directly to the triazine series. The active site of *TgCPL* contains four residues (**Figure 4A**) that are either non-conserved across the human cathepsin isoforms A-X, or unique to *TgCPL*. Notably, the S3 pocket of *TgCPL* tends to be significantly more polar as compared to *HsCPL*, with Gln69, Asp78, and Glu75 making up the key pocket residues. The human cathepsin L (**Figure 4B**) is somewhat more lipophilic with the S3 pocket residues Glu63, Tyr72 and Leu69, respectively. While this presents potential for differences in ligand selectivity, the S3 pocket is shallow and somewhat promiscuous with its preferred residues. We anticipated that the majority of our potential selectivity would come from the S2 pocket, which tends to be deeper and somewhat more defined. Importantly, the parasitic cathepsin bears an Asp218 in the S2 pocket, while the human isoform contains an Ala214 in the

1
2
3 corresponding position. We therefore expected that selectivity for *TgCPL* could be achieved by exploiting
4
5 the differences in the overall topology and unique residues. As such, we chose to explore various P2 and
6
7 P3 vectors to probe these differences and elucidate the pharmacophore for selective and potent inhibition of
8
9 *TgCPL*.

14 SAR of P3 Vectors

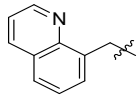
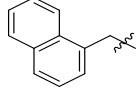
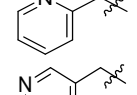
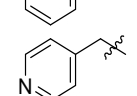
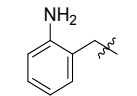
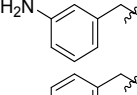
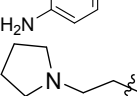
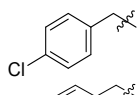
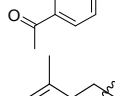
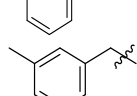
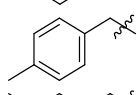
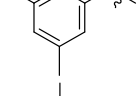
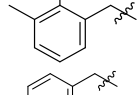
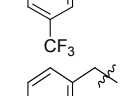
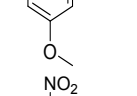
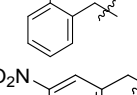
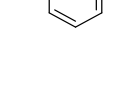
17 **Table 1.** SAR of P3 vectors

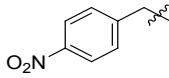
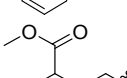


28
29
30
31
32
33
34
35
36
37
38
39
40
41
42
43
44
45
46
47
48
49
50
51
52
53
54
55

No.	R	<i>TgCPL</i> ^a IC ₅₀ (nM)	<i>HsCPL</i> ^b IC ₅₀ (nM)	Selectivity for <i>TgCPL</i> ^c
HTS Lead 3	see Fig 1	3,500	2,300	0.7
4		34	32	0.9
5		47	20	0.4
6		53	19	0.4
7		356	33	0.09
8		53	34	0.6
9		48	35	0.7
10		101	62	0.6
11		110	86	0.8
12		230	35	0.2

1
2
3
4
5
6
7
8
9
10
11
12
13
14
15
16
17
18
19
20
21
22
23
24
25
26
27
28
29
30
31
32
33
34
35
36
37
38
39
40
41
42
43
44
45
46
47
48
49
50
51
52
53
54
55
56
57
58
59
60

1					
2					
3					
4	13		61,457	12	0.0002
5					
6					
7	14		15,200	2	0.001
8					
9					
10	15		82	33	0.4
11					
12	16		39	27	0.7
13					
14					
15	17		107	41	0.4
16					
17	18		230	87	0.4
18					
19					
20	19		95	28	0.3
21					
22	20		137	296	2.2
23					
24	21		304	492	1.6
25					
26					
27	22		32	6	0.2
28					
29	23		95	36	0.4
30					
31	24		107	14	1.3
32					
33					
34					
35	25		64	22	0.3
36					
37	26		19	5	0.3
38					
39					
40	27		37	41	1.1
41					
42					
43	28		17	47	2.8
44					
45					
46	29		17	3	0.2
47					
48					
49	30		47	6	0.1
50					
51					
52	31		27	96	3.6
53					
54					
55	32		42	14	0.3
56					
57					
58					
59					
60					

33		59	51	0.9
34		105	56	0.5
35		740	266	0.4
36		123	91	0.7
37		970	67	0.07
^{a,b} IC ₅₀ for <i>Toxoplasma gondii</i> Cathepsin L (<i>TgCPL</i>) or human Cathepsin L (<i>HsCPL</i>). Values are mean of at least 3 independent experiments with SEM typically < 30%. ^c Selectivity for <i>Toxoplasma gondii</i> Cathepsin L as defined by the ratio <i>HsCPL</i> IC ₅₀ / <i>TgCPL</i> IC ₅₀				

We began our SAR investigation by retaining the isoamyl P2 vector and varying the P3 position (**Table 1**). A scan of fluorine mono-substitution of the P3 benzyl (**5** and **6**) showed retention of activity, but no significant improvement in either overall potency or selectivity. A similar outcome was seen with the P3 di-fluoro analogs **7**, **8**, and **9**. The non-fluorinated P3 benzyl pendant **10** exhibited roughly a 3-fold loss of potency versus the 4-fluoro lead **4**. Homologation of the linker from methyl to ethyl (**11**) or propyl (**12**), while better tolerated for the human isoform, resulted in the same reduced potency for *TgCPL*. An even greater loss of potency for the parasitic enzyme was seen when large bulky pendants like the quinoline or naphthyl of **13** and **14** were installed. Taken together, this demonstrates that the parasitic isoform does not productively accommodate large lipophilic vectors in the P3 position, which is consistent with the topologically more polar nature of the S3 pocket defined by Asp78 and Glu75 (**Figure 4A**).

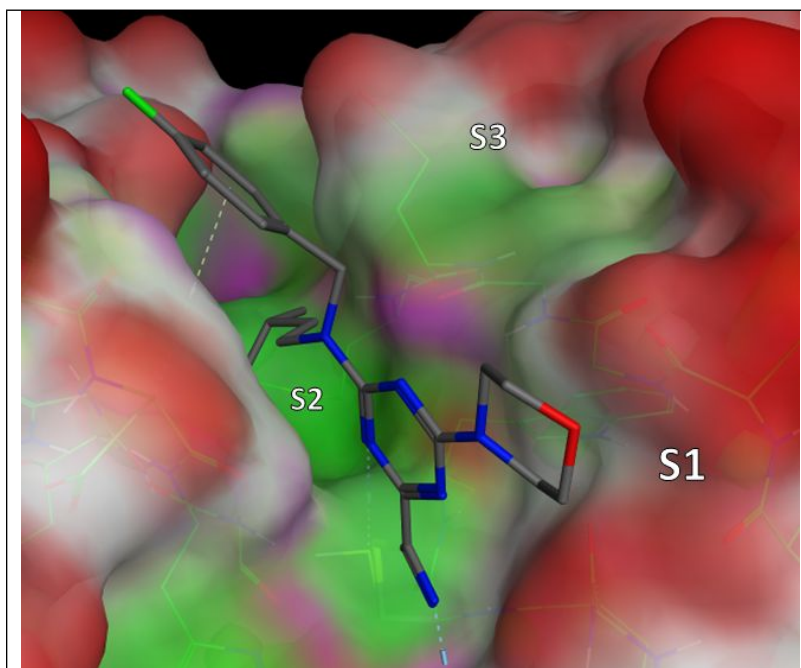
With this in mind, we tried the 2-, 3-, and 4-pyridyl pendants (**15**, **16**, and **17**) in P3, with the objective of improving our selectivity for the parasite, as well as potentially improving our metabolic profile by decreasing the clogP. Of these, the 3-pyridyl (**16**) retained potency, but unfortunately did not offer any improvement in selectivity over the human isoform. Anilines **18**, **19**, and **20** were also evaluated. We had hoped to gain a meaningful interaction with Asp78, Gln69, or Glu75 in *TgCPL*

1
2
3 (Figure 4A), but none of the anilines were very potent for *TgCPL*. However, analog **20** did afford a small
4 measure of selectivity toward *TgCPL* (*HsCPL* IC₅₀/*TgCPL* IC₅₀ = 2.2). Analog **21** was tested to determine
5 if a basic amine might afford greater *TgCPL* selectivity, but resulted in nearly a 9-fold loss in potency
6 versus parent compound **4**.
7
8
9

10
11
12
13
14 As a comparison to our 4-fluorobenzyl pendant, we tested the 4-chlorobenzyl analog **22** to
15 determine the impact of a larger halogen. While equally effective against *TgCPL* to the 4-fluoro, this
16 change afforded an order of magnitude improvement in potency for *HsCPL*. Analog **23** was synthesized
17 to assess the effects of a moderately electron withdrawing acetophenone, but afforded a mild reduction in
18 potency against *TgCPL*. A methyl scan was performed to probe the space around the ring and determine if
19 any of the substitution patterns might lead toward some selectivity for *TgCPL*. While **24** and **25** did not
20 offer any improvement in potency, **26** was nearly twice as potent (*TgCPL* IC₅₀ = 19 nM) as the parent
21 scaffold **4**, but more strongly improved *HsCPL* inhibition (*HsCPL* IC₅₀ = 5 nM), similar to what we
22 observed with the 4-chloro analog **23**. It is worth noting that the *o*-methyl benzyl analog **24**, while less
23 potent than the 4-fluorobenzyl, showed mild selectivity for *TgCPL*. Dimethyl analogs **27** and **28** provided
24 more potent inhibitors and were consistent with the trend that an ortho substitution (**28**) may favor
25 selectivity for *TgCPL*. Undesirably, these also increased overall molecular weight and introduced
26 potential metabolic hotspots, and therefore were not further pursued. The electron withdrawing 3-
27 trifluoromethyl **29** provided one of the more potent *TgCPL* inhibitors (IC₅₀ = 17 nM), but exhibited
28 selectivity in favor of *HsCPL*. The increased MW versus **4** was also undesirable in trying to remain
29 within the calculated properties for BBB permeability. The corresponding 3-methoxy analog **30** was also
30 tested to assess the effects of electron donation into the ring; however, this did not seem to offer any
31 significant improvement in potency or selectivity as compared to **29**. Interestingly, a nitro scan in analogs
32 **31**, **32**, and **33** revealed that the *o*-nitrobenzyl P3 vector of **31** exhibited a 3-fold selectivity over the
33 human isoform (*TgCPL* IC₅₀ = 27 nM, *HsCPL* IC₅₀ = 96 nM), consistent with the modest selectivity we
34 observed with ortho-methyl analogs **24** and **28**. As this was the most *TgCPL*-selective analog to date,
35
36
37
38
39
40
41
42
43
44
45
46
47
48
49
50
51
52
53
54
55
56
57
58
59
60

1
2
3 additional ortho-substituted analogs **34**, **35**, **36**, and **37** were synthesized in an effort to better explain the
4 observed selectivity. The nitrile (**34**), trifluoromethyl (**35**), and methyl ester (**35**) vectors were tested as
5 isosteres of the nitro. Unfortunately, none of these substituents reproduced the selectivity we saw with the
6 *o*-nitro vector. The *o*-methoxy analog **37** was also synthesized to determine if the observed effects were
7 due to the electron withdrawing nature of the nitro, or a conformational change due to sterics. While
8 tolerated in *HsCPL*, the potency significantly decreased against *TgCPL*.
9
10
11
12
13
14
15

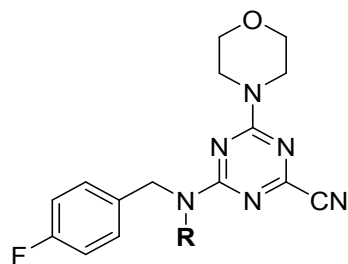
16 Based on observations in our modeling (**Figure 5**), we hypothesize that the P3 pendant may have
17 the ability to bind outside of the S3 pocket and interact with the backbone of Asp166, giving rise to a
18 higher tolerance for vectors as compared to that of S2. This concept is supported by the overall lack of
19 robust SAR trends for the S3 pocket and the relatively high substrate tolerance in the P3 position observed
20 in analogs **4-47**. Furthermore, a recent publication observed a similar trend in triazine nitrile inhibitors of
21 human cathepsin L.³¹
22
23
24
25
26
27



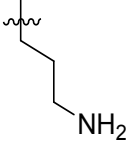
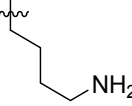
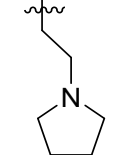
28
29
30
31
32
33
34
35
36
37
38
39
40
41
42
43
44
45
46
47
48
49
50 **Figure 5.** Potential alternative binding mode for triazine nitriles
51 (e.g. **4**). Derived from PDB: 3F75
52
53
54
55
56
57
58
59
60

SAR Analysis of P2 Vectors:

Table 2. Screen of various P2 vectors



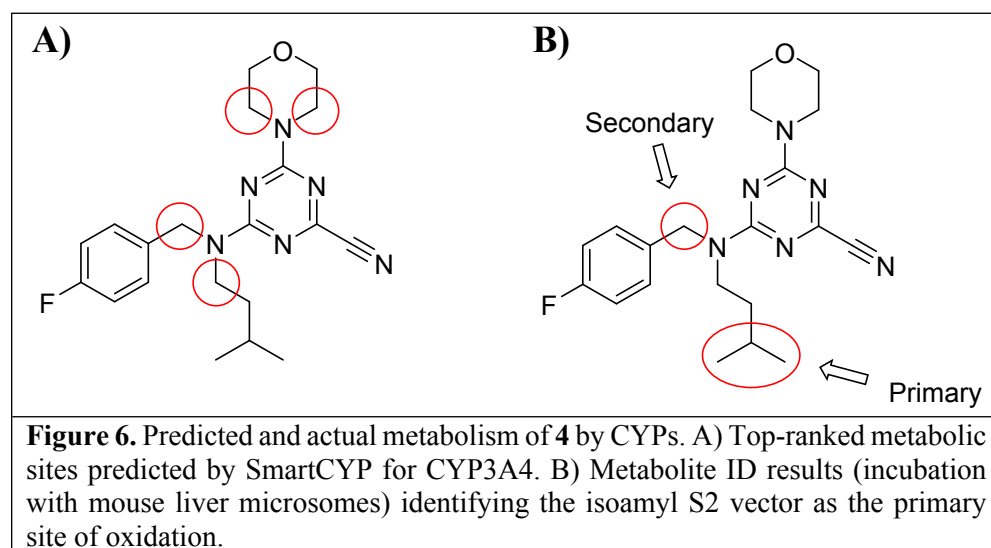
No.	R	<i>TgCPL</i> ^a IC ₅₀ (nM)	<i>HsCPL</i> ^b IC ₅₀ (nM)	Selectivity for <i>TgCPL</i> ^c
4		34	32	0.94
38		246	67	0.27
39		117	26	0.22
40		144	64	0.44
41		46	32	0.70
42		67	2	0.030
43		220	328	1.5
44		2,260	759	0.33
45		6,490	3,430	0.52

46		3,590	4,090	1.1
47		1,410	561	0.40
48		1,990	2,050	1.1

^{a,b}IC₅₀ for *Toxoplasma gondii* Cathepsin L (*TgCPL*) or human Cathepsin L (*HsCPL*).
 Values are mean of at least 3 independent experiments with SEM typically < 30%.
^cSelectivity for *Toxoplasma gondii* Cathepsin L as defined by the ratio *HsCPL* IC₅₀/*TgCPL* IC₅₀

We then turned our attention to evaluating the SAR among the postulated S2 vectors. In general, the papain family of proteases achieve their substrate specificity primarily from interactions in the S2 pocket.³⁸ Based on our previous SAR studies with the dipeptide nitriles, we had determined that leucine was the optimal amino acid for the P2 position. As already noted with **4**, the isoamyl sidechain in the respective position for the triazine nitriles afforded a huge improvement in potency to HTS lead **3** (*TgCPL* IC₅₀ = 34 nM). We wanted to first determine if the previous dipeptide SAR trends we found tracked in a similar fashion with this new chemotype. Initially, we evaluated the effects of shorter, aliphatic vectors. The n-propyl, n-butyl, and n-butenyl (**38**, **39**, and **40**) were tolerated in *HsCPL*, but all decreased in potency for *TgCPL*. Consistent with our previous SAR, the shorter isobutyl S2 vector in **42**, which closely mimics a valine sidechain, slightly decreased activity for *TgCPL* to 67 nM, but enhanced *HsCPL* inhibition (IC₅₀ = 2 nM). Interestingly, the dehydroleucine analog **41** retained nearly equivalent potency (*TgCPL* IC₅₀ = 46 nM) to **4**, a trend that was not observed in the previous dipeptide series. This indicated to us that, while similar, the SAR between the dipeptide and triazine chemotypes was not identical and that binding of the triazine nitrile series may be somewhat better accommodated by the enzyme. Extension of the S2 sidechain of **4** by one carbon in **43** resulted in a significant loss of potency. We believe this may be due to a clash in the back of the S2 pocket, consistent with the S2 size constraints observed previously.²⁸ Compound **44** was made to determine if the S2 pocket could tolerate a less lipophilic group

thereby reducing overall clogP and improving compound solubility. Unfortunately, this resulted in a large decrease in potency for both enzymes. Given that *TgCPL* bears a unique Asp218 versus the Ala214 in *HsCPL* (**Figure 4**), we rationalized that inclusion of a basic group in the S2 position might afford some selectivity, as well as improve compound solubility. As such, compounds **45-48** were synthesized. We had hoped that the stepwise increase in side chain length might elucidate the ideal distance required to gain a productive interaction with Asp218. Unfortunately, these changes were not well tolerated and resulted in a drastic drop in potency down to the low micromolar range for both enzymes, indicating that perhaps these compounds are not binding as predicted, or that Asp218 is not oriented the way it appears in our model.

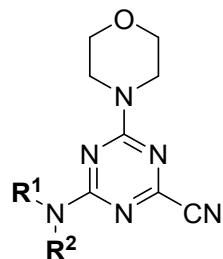


P2 Vectors for Improved Metabolic Profile and Selectivity:

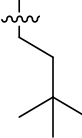
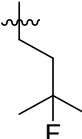
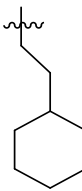
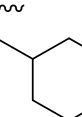
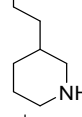
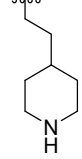
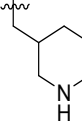
The previously developed dipeptide nitrile **2** exhibited a fair level of stability toward mouse liver microsomes (MLM) with a half-life of $t_{1/2} = 22$ min. While the scaffold hop from dipeptide **2** to the triazine nitrile **4** resulted in an improvement in both potency and predicted CNS profile, it also imparted a significant drop in metabolic stability (MLM $t_{1/2} = 7$ min). The metabolic liabilities predicted by SmartCyp (**Figure 6A**) led us to install the α -methyl and exchange the P1 solubilizing group with 3-

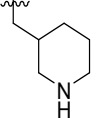
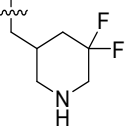
amino-oxetane in analog **50** (Table 3). Unfortunately, this did not offer any improvement to the microsomal stability profile (MLM $t_{1/2}$ = 5 min). Therefore, a metabolite ID study was performed to experimentally determine sites of oxidative metabolism. As shown in Figure 6B oxidation of **4** occurs predominantly on the P2 isoamyl vector and the P3 benzylic methylene. Similar oxidation of S2 isoamyl sidechains has been reported in the development of odanacatib for the inhibition of cathepsin K, and it was overcome by replacement of the sidechain with fluoroleucine.³⁹ With this guidance in mind, analogs were designed to retain the physiochemical profile of a CNS drug and simultaneously circumvent these potential metabolic liabilities (Table 3).

Table 3. P2 Vectors for Improved Metabolic profile and Selectivity



No.	R ¹	R ²	<i>TgCPL</i> ^a IC ₅₀ (nM)	<i>HsCPL</i> ^b IC ₅₀ (nM)	Selectivity for <i>TgCPL</i> ^c	MLM $t_{1/2}$ (min)
4	4-Fluorobenzyl		34	32	0.94	7
49	4-Fluoro- α -methylbenzyl		26	15	0.58	
50*	4-Fluoro- α -methylbenzyl		92	23	0.25	5
51	4-Fluorobenzyl		310	190	0.61	
52	4-Fluoro- α -methylbenzyl		143	103	0.72	4.4

1							
2							
3							
4							
5	53	4-Fluorobenzyl		68	160	2.4	
6							
7							
8							
9	54	4-Fluorobenzyl		17	26	1.5	3.5
10							
11							
12							
13							
14	55	4-Fluorobenzyl		66,800	87,500	1.3	
15							
16							
17							
18	56	4-Fluorobenzyl		26	95	3.7	15
19							
20							
21	57	4-Fluorobenzyl		3,570	66	0.018	
22							
23							
24	58	4-Fluorobenzyl		110	77	0.70	
25							
26							
27	59	4-Fluorobenzyl		74	60	0.81	
28							
29							
30	60	4-Fluorobenzyl		1,900	1,190	0.63	
31							
32							
33	61	4-Fluorobenzyl		326	969	2.9	
34							
35							
36	62	4-Fluorobenzyl		181	1,200	6.7	>60
37							
38							
39	63	4-Fluorobenzyl		1,200	960	0.80	
40							
41							
42	64	4-Fluorobenzyl		400	94	0.25	
43							
44							
45	65	4-Fluorobenzyl		49	170	3.5	3.5
46							
47							
48							
49							
50							
51							
52							
53							
54							
55							
56							
57							
58							
59							
60							

66	4-Fluorobenzyl		630	370	0.58
67	2-Nitrobenzyl		3,970	1,240	0.3
68	4-Fluorobenzyl		1,600	517	0.33

^{a,b}IC₅₀ for *Toxoplasma gondii* Cathepsin L (*TgCPL*) or human Cathepsin L (*HsCPL*). Values are mean of at least 3 independent experiments with SEM typically < 30%. ^cSelectivity for *Toxoplasma gondii* Cathepsin L as defined by the ratio *HsCPL* IC₅₀/*TgCPL* IC₅₀. *S1 morpholine group replaced with oxetan-3-amine.

Analog **49** was prepared first to evaluate the impact of the alpha-methylbenzyl on potency since we had previously observed a loss of potency with oxetane analog **50**. In fact this single change was well tolerated and provided a small improvement in overall potency; however, the potency improvement was 2-fold greater for *HsCPL*. Presumably due to the added MW and lipophilicity, compound solubility significantly decreased versus the parent compound (thermodynamic aqueous solubility: **4** = 42 μM, **49** = 16 μM). In an effort to resolve this, we tried replacing the S1 morpholine group with oxetanamine in analog **50**. As noted previously, the potency decreased to 92 nM for *TgCPL*, but solubility improved to 42 μM. Analogs **51**, **53**, and **54** were all synthesized with the intent of blocking oxidation of the isoamyl CH.³⁹⁻⁴⁰ The cyclopropyl leucine mimic (**51**) lost an order of magnitude in potency (*TgCPL* IC₅₀ = 310 nM) compared to **4**, and the t-butyl analog, **53**, while 2-fold selective for *TgCPL*, decreased to 68 nM against *TgCPL*. It should be noted, however, that these respective changes in the dipeptide nitrile series were not tolerated nearly as well, giving us some confidence that the triazine nitrile may be a superior scaffold with regards to potential for improving PK properties. Furthermore, this data suggests these two chemotypes are not binding in precisely the same manner, consistent with what we had observed earlier in our SAR. Compound **52** was synthesized to determine if the cyclopropyl and α-methylbenzyl combination in P2 and P3 respectively would be sufficient to slow metabolism. Unfortunately, this actually decreased the MLM t_{1/2} to 4.4 min, indicating a likely switch to another metabolic site, perhaps

1
2
3 N-dealkylation of the P2 sidechain or oxidation of the P1-morpholine. Compound **54**, bearing a
4 fluoroleucine in S2 (a vector also not tolerated in the dipeptide series), demonstrated excellent potency for
5 *TgCPL* ($IC_{50} = 17$ nM) and *HsCPL* ($IC_{50} = 26$ nM), although MLM stability was decreased to $t_{1/2} = 3.5$
6 min, further indicating that blocking the primary metabolic site alone is insufficient for improving
7 stability. The ethyl-cyclohexyl vector of **55** resulted in a significant decrease in potency for both
8 cathepsins, likely due to the same steric clash in the S2 pocket observed for compound **43**. Interestingly,
9 *shortening the pendant by one carbon to the methyl-cyclohexyl (56) both retained potency for TgCPL*
10 ($IC_{50} = 26$ nM) and achieved nearly 4-fold selectivity for the parasite isoform over human. Furthermore,
11 it doubled the MLM $t_{1/2}$ of lead **4** to 15 min. The P2 cyclopentyl in **59** is comparable to the cyclohexyl in
12 terms of potency, but not as selective. The smaller ring sizes in analogs **57** and **58** significantly decreased
13 potency for *TgCPL* and were not further pursued.

14
15
16
17
18
19
20
21
22
23
24
25
26
27
28
29
30
31
32
33
34
35
36
37
38
39
40
41
42
43
44
45
46
47
48
49
50
51
52
53
54
55
56
57
58
59
60

Given the favorable *TgCPL* selectivity imparted by the P2 cyclohexyl ring for **56**, we also explored incorporation of a basic amine with the objective of enhancing this selectivity through a favorable ionic interaction with Asp218. As such, S2 piperidinylmethyl compounds **62** and **63** were synthesized. Interestingly, the 4-piperidine of **63** resulted in sharply reduced activity against both enzymes, while the 3-piperidine **62** demonstrated good selectivity (7-fold) for *TgCPL*. Despite a decrease in overall potency to 0.180 μ M, **62** exhibited a much improved MLM stability with $t_{1/2} > 60$ minutes. The drastic improvement in stability seen for compound **62** is likely due to the added charge of the basic amine impeding CYP binding. The addition of an extra carbon in the sidechain for analog **60** decreased potency to 1.9 μ M for *TgCPL*, consistent with the poor activity of the homologated cyclohexane analog **55**. The ethyl 4-piperidine P2 vector **61** showed a slightly improved potency as compared to analog **60**, however it was still significantly lower than parent analog **56**. The respective tetrahydropyran analogs **64** and **65** were made to determine if the basic amine was important for this observed selectivity. These displayed a similar potency and selectivity profile, with the heteroatom being better tolerated at the 3-position (**65**, *TgCPL* $IC_{50} = 49$ nM) than the 4-position (**64**, *TgCPL* $IC_{50} = 400$ nM). Unfortunately,

1
2
3 compound **65** was not stable to MLM. Reduction of the piperidine ring size to a pyrrolidine in analog **66**
4
5 abolished the selectivity and potency profile. Finally, we attempted to combine our most selective P2 (3-
6
7 piperidinylmethyl) and P3 (*o*-nitro benzyl) vectors with analog **67**. Unfortunately, these effects were not
8
9 synergistic and resulted in a loss of both selectivity and potency, strongly suggesting that the two
10
11 congeners are not binding the same way.
12
13

14 15 16 **Pharmacokinetics:**

17
18 Compound **4** was evaluated in a mouse PK study to benchmark the CNS profile of the triazine
19
20 nitrile chemotype and compare it to that of the dipeptide nitrile **2** (**Table 4**). We were pleased to find that
21
22 **4** does in fact access the CNS with a brain AUC/plasma AUC = 0.61. However, the compound levels
23
24 decreased rather quickly, likely due to a combination of high volume of distribution and metabolic
25
26 instability. Nonetheless, this was a promising result indicating that the triazine nitrile scaffold has the
27
28 physiochemical profile needed to cross the blood-brain barrier.
29
30
31
32

33 **Table 4.** Pharmacokinetic studies in mice*

No.	[Plasma] (ng/mL)				[Brain] (ng/g)				AUC _{Brain} (ng*hr/g)	AUC _{Plasma} (ng*hr/mL)	AUC _{Brain} / AUC _{Plasma}
	0.5	2	4	7	0.5	2	4	7			
2	110	138	10.2	-	53.6	-	-	-	53.6	376	0.14
4	141	17.3	7.4	3.1	90.8	16.1	-	-	119	195	0.61
50	1,530	57.7	4.7	11.4	671	82.5	12.5	13.8	868	1660	0.52
62	473	200	65.9	14.3	36.1	32	16.6	12.4	152	1010	0.15

41 * Compounds were administered as a single IP dose at 10 mg/kg.
42
43

44 We hoped that by increasing the metabolic stability of the scaffold, we might gain a better
45
46 pharmacokinetic profile. We attempted to evaluate compound **56**, as this analog exhibited an improved
47
48 half-life *in vitro*, good potency, and demonstrated some selectivity for TgCPL, but unfortunately its poor
49
50 solubility precluded *in vivo* dosing. As mentioned above, the replacement of the P1 morpholine of **49** with
51
52 a 3-amino-oxetane in compound **50** offered an improvement in solubility (16 μ M to 42 μ M respectively).
53
54 We decided to perform a PK study on **50** to determine if the additional hydrogen bond donor of the
55
56
57
58
59
60

1
2
3 oxetanamine would impede our CNS penetrance, or if this could be a viable strategy to improve the
4 solubility of future compounds (**Table 4**). We were very pleased to find that in addition to retaining CNS
5 access, the overall exposure levels were significantly increased compared to **4**. Given that the 3-piperidine
6 P2 vector in **62** significantly improved the metabolic stability, we also evaluated its pharmacokinetic
7 profile. While the exposure levels were improved in plasma versus **4**, this compound had markedly
8 reduced BBB penetrance. Basic amines are often associated with efflux by Pgp, so the difluoro-3-
9 piperidine compound **68** was synthesized with the intent of attenuating the basicity of this sidechain
10 (**Table 3**). Unfortunately, this change was not well tolerated and potency was reduced to low micromolar
11 for this compound ($TgCPL\ IC_{50} = 1.6\ \mu M$).
12
13
14
15
16
17
18
19
20
21
22
23

24 Because of their markedly divergent brain:plasma ratios observed in the PK studies, compounds
25 **50** and **62** were assessed *in vitro* to determine whether they are potential substrates of P-glycoprotein (P-
26 gp). Evaluation in an MDR1/MDCK permeability assay indicated that compound **50** has high passive
27 permeability and an efflux ratio <1, and thus does not appear to be a Pgp substrate (**Table 5**). This would
28 be expected to translate to good CNS penetrance, which is in agreement with our PK results. **62** also
29 demonstrated high passive permeability, but has an efflux ratio of over 17, indicating this compound is
30 likely a P-gp substrate, explaining its poor brain exposure *in vivo*. As noted above, this is very likely to be
31 due to the presence of the basic amine in **62**.
32
33
34
35
36
37
38
39
40
41
42

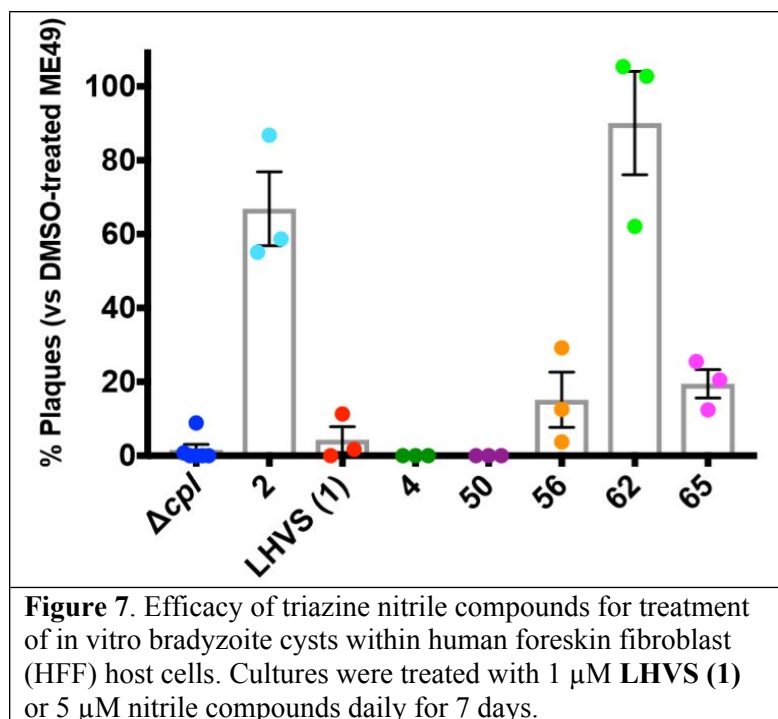
43 **Table 5.** MDR1/MDCK Assay results

Sample	P_{app}^a (cm/sec)	Efflux Ratio (B-A)/(A-B)
50 (A-B)	3.55×10^{-5}	0.223
50 (B-A)	7.92×10^{-6}	
62 (A-B)	2.59×10^{-5}	17.2
62 (B-A)	4.47×10^{-4}	
^a Values shown are the average of two sample measurements of the acceptor wells from three replicate assays.		

44
45
46
47
48
49
50
51
52
53
54
55
56
57
58
59
60

In vitro efficacy studies:

Based on their potencies vs TgCPL, five compounds were selected for evaluation of their effects on plaque formation in a *T. gondii* bradyzoite cyst qPCR/plaque viability assay in vitro (**Figure 7**). This assay involves isolating bradyzoites after treatment and quantifying viability by applying them to a new monolayer of host cells. Viable bradyzoites invade the monolayer, differentiate to tachyzoites, and form a visible plaque after 12 days of growth. Viability is calculated as the number of plaques/1000 genomes of input bradyzoites (measure by qPCR) and expressed as a percentage of solvent (DMSO) treated bradyzoite cysts. Positive controls in the assay included a TgCPL knockout strain of *T. gondii* (Δcpl), as well as the irreversible TgCPL inhibitor LHVS (**1**)²⁵. We were pleased to find that the triazine nitriles **4** and **50** exhibited strong efficacy at 5 μ M that was equivalent to the genetic knockout and irreversible inhibitor LHVS at 1 μ M, with zero plaques formed in any biological replicate. *To our knowledge, this is the first example of a reversible inhibitor of TgCPL achieving in vitro efficacy against the chronic (bradyzoite) stage of T. gondii.* Triazine nitrile analogs **56**, **65**, and **62**, on the other hand, showed variable efficacy. **56** and **65** were slightly less efficacious than **4** and **50** at the concentration tested, reducing cyst viability by ~80% across three biological replicates. Only one biological replicate of compound **62** reduced viability (<20%), suggesting that it was comparatively ineffective. Dipeptide nitrile lead (**2**) demonstrated only modest activity against the bradyzoite cysts, exemplifying the improved potential of the triazine nitrile as a therapeutic.



To confirm that the observed reduction in bradyzoite viability was not due to human foreskin fibroblast (HFF) host cell viability being indirectly compromised, MTS assays were also conducted to assess cell cytotoxicity (CC). The relatively high CC_{50} values indicate that none of the compounds would be expected to cause significant host cell cytotoxicity at the concentration used in the qPCR/plaque bradyzoite cyst viability assays (5 μM).

Table 6. MTS assay results in HFF cells.

Compound	CC_{50} (μM) ^a
4	65.19 (± 16.69)
50	29.05 (± 2.6)
56	>100
62	61.05 (± 2.08)
65	34.58 (± 1.33)

^aAll values are the mean of at least three independent experiments.

CONCLUSIONS AND PERSPECTIVES

1
2
3 Throughout this project, significant advances have been made in developing small molecule
4 inhibitors of *TgCPL*. We have elucidated key SAR for the inhibition of *TgCPL*, developed potent and
5 CNS penetrant inhibitors, and demonstrated efficacy against bradyzoite cysts in vitro. We started by
6 conducting a high throughput screen to identify new chemotypes capable of the inhibition of *Toxoplasma*
7 *gondii* cathepsin L as potential new therapeutics for toxoplasmosis. The low μM triazine nitrile scaffold
8 (**3**) was selected based on the previously established literature precedent of this chemotype for inhibition
9 of human cathepsins, its low molecular weight, and physical properties consistent with CNS-active
10 compounds. Translation of the pharmacophore previously developed with our dipeptide nitrile series to
11 the triazine nitrile scaffold resulted in an immediate 100-fold gain in potency (*TgCPL* IC_{50} = 34 nM), but
12 reduced metabolic stability relative to the corresponding dipeptide. A *TgCPL* covalent docking model was
13 developed using the crystal structure of *TgCPL* and the crystal structure(s) of human cathepsin (*HsCPL*)
14 in complex with various dipeptide and triazine nitrile inhibitors. Using this we were able to identify key
15 distinctions between the parasite and human isoforms of cathepsin L. In particular, the smaller S2 pocket
16 and the four unique residues (Asp218, Glu75, Asp78, and Gln69) were targeted with the goal of gaining
17 selectivity for *TgCPL*. 68 analogs in this series were synthesized with varying S2 and S3 vectors to
18 optimize metabolic stability, CNS permeability, and selectivity over human isoforms. In general, we
19 found that variations in the P3 position had little impact on potency or selectivity. As expected, the bulk
20 of the potency and selectivity seems to be imparted by efficient binding in the S2 position. The S2 pocket
21 across the human cathepsins tends to be more uniformly lipophilic than *TgCPL*, and we predicted that
22 inclusion of a basic residue in the P2 position might interact favorably with non-conserved Asp218 in
23 *TgCPL*. It is worth noting that out of the nine analogs bearing an amine in P2, all exhibited IC_{50} s for
24 *HsCPL* of $>0.5 \mu\text{M}$, supporting that the human isoform does not tolerate a basic amine in S2. *TgCPL*,
25 conversely, appears to be able to better accommodate either a nitrogen or oxygen in S2, likely due to the
26 polar Asp218 residue in the back of the S2 pocket, and this may represent an avenue for further *TgCPL*
27 selectivity enhancement. Work in our laboratory is underway to exploit these features and further explore
28 the SAR trends with various basic and polar groups in P2.
29
30
31
32
33
34
35
36
37
38
39
40
41
42
43
44
45
46
47
48
49
50
51
52
53
54
55
56
57
58
59
60

1
2
3 Overall, we improved potency against *TgCPL* to as low as 5 nM and identified features that can
4 be exploited to gain selectivity vs *HsCPL* (up to 5-7 fold), and significantly improved metabolic stability
5 (up to $t_{1/2} > 60$ min in MLM). Importantly, we were able to demonstrate significant brain penetration with
6 several analogs in vivo in mice. Although our most *Tg*-selective analog **62** bearing a basic amine in the P2
7 pendant proved to be highly susceptible to efflux in MDR1-MDCK cells in vitro and demonstrated low
8 brain exposure in vivo, an analog lacking this basic amine (**50**) was shown not to be a P-gp substrate and
9 achieved good exposure in the brains of mice after IP dosing, suggesting the triazine nitrile chemotype
10 has promise as an in vivo probe for chronic *T. gondii* infection studies. Synthesis of new analogs to
11 further improve PK and isoform selectivity are underway. Finally, we demonstrated for the first time that
12 in vitro treatment of *T. gondii* bradyzoite cysts with non-peptidic triazine nitrile inhibitors reduces
13 parasite viability with efficacy equivalent to a *TgCPL* genetic knockout, in contrast to one of our
14 previously developed dipeptide nitriles, highlighting the increased therapeutic potential of the triazine
15 template. This is the first example of a CNS penetrant, reversibly covalent *TgCPL* inhibitor showing
16 efficacy in an in vitro model of bradyzoite stage parasites. Current studies are underway to advance the
17 triazine nitrile series into an *in vivo* model of latent *Toxoplasma* infection.
18
19
20
21
22
23
24
25
26
27
28
29
30
31
32
33
34
35
36
37

38 METHODS

39
40
41 **Chemistry General Information:** All reagents were used without further purification as received from
42 commercial sources unless noted otherwise. ^1H NMR spectra were taken in DMSO-*d*₆, MeOD, or CDCl₃
43 at room temperature on Varian Inova 400 MHz or Varian Inova 500 MHz instruments. Reported chemical
44 shifts for the ^1H NMR and ^{13}C NMR spectra were recorded in parts per million (ppm) on the δ scale from
45 an internal standard of residual tetramethylsilane (0 ppm). Mass spectrometry data were obtained on either
46 a Micromass LCT or Agilent Q-TOF. An Agilent 1100 series HPLC with an Agilent Zorbax Eclipse
47 Plus-C18 column was used to determine purity of biologically tested compounds. Unless otherwise noted,
48 all tested compounds were determined to be >95% pure using a 6 minute gradient of 10-90% acetonitrile
49
50
51
52
53
54
55
56
57

1
2
3 in water followed by a 2 minute hold at 90% acetonitrile with detection at 254 nm. Flash chromatographic
4 purifications were performed using a Teledyne ISCO Combiflash RF with Redisep Gold RF columns.
5
6
7

8 9 **General Procedure A1: Reductive Amination**

10
11 To a dry round bottom flask with DCM was added aryl aldehyde or aryl ketone **Int-1a** (1 eq),
12 followed by the addition of the desired primary amine (1 eq), final reaction concentration of 0.1-0.3 mM.
13
14 The vessel was then stirred under a nitrogen atmosphere at room temperature overnight. Sodium
15 triacetoxyborohydride (3 eq) was then added and reaction was stirred at room temperature for 1-3 hr. The
16 reaction was quenched slowly with water then poured into water and extracted 3x with DCM. The
17 combined organic layer was dried over sodium sulfate and concentrated *in-vacuo*. The crude product was
18 further purified by column chromatography (0-10% MeOH in DCM + 0.1% TEA) to afford the desired
19 secondary amine **Int-2a**.
20
21
22
23
24
25
26
27
28
29

30 31 **General Procedure A2: S_NAr**

32
33 Under a dry nitrogen atmosphere, cyanuric chloride (1 eq) was added a roundbottom flask along
34 with DCM (final conc. = 0.1-0.3 mM). The vessel was cooled to -10°C (Ice/Brine) and the desired
35 secondary amine (1 eq) and DIPEA (1 eq) were then added. Reaction was stirred at -10°C for 1 h. The
36 reaction was poured into water and extracted 3x with DCM. Combined organic layers were dried over
37 MgSO₄ and concentrated in vacuo. The crude product was further purified by column chromatography (0-
38 100% EtOAc in Hexanes gradient) to afford the desired intermediate **Int-3a**.
39
40
41
42
43
44
45
46
47

48 49 **General Procedure A3: S_NAr**

50
51 Under a dry nitrogen atmosphere, dichloro triazine intermediate (1 eq) was added a roundbottom
52 flask along with DCM to a final reaction concentration of 0.1 mM. The vessel was cooled to -10°C
53 (Ice/Brine) and DIPEA (1 eq) and morpholine (1 eq) were then added. Reaction was stirred and allowed
54 to warm to room temperature over 6-12 h. The reaction was poured into water and extracted 3x with
55
56
57
58
59
60

1
2
3 DCM. Combined organic layers were dried over MgSO₄ and concentrated in vacuo. The crude product
4 was further purified by column chromatography (0-100% EtOAc in Hexanes gradient) to afford the
5 desired intermediate **Int-4a**.
6
7
8
9

10 11 **General Procedure A4: Cyanation**

12
13 A dry pressure vessel was charged with the appropriate triazinyl chloride (1.0 eq), and suspended
14 in DMSO/H₂O 9:1. KCN (1.1 eq.) and 1,4-diazabicyclo[2.2.2]octane (DABCO, 2.0 eq.) were added and
15 the reaction was heated to 80°C. Reaction was left to stir at this temperature until LC/MS showed
16 completion of the reaction (6-12 h). Reaction was cooled to room temperature, diluted with EtOAc, and
17 washed thoroughly with brine (3-5 x). The organic layer was separated, dried over MgSO₄, filtered, and
18 evaporated. The crude product was further purified by column chromatography (0-100% EtOAc in
19 Hexanes gradient) to afford the desired product.
20
21
22
23
24
25
26
27
28
29

30 31 **General Procedure B1: One-pot double S_NAr**

32 Under a dry nitrogen atmosphere, cyanuric chloride (1 eq) was added a roundbottom flask along
33 with DCM (final conc. = 0.1-0.3 mM). The vessel was cooled to -10°C (Ice/Brine) and DIPEA (1 eq)
34 followed by the desired primary amine **Int-1b** (1eq) were then added. Reaction was stirred at for 1-3 hr,
35 until TLC/HPLC indicated substitution was complete. Next, DIPEA (1 eq) was added followed by
36 morpholine (1 eq) and reaction was allowed to stir and warm to rt over 4-12h until TLC/HPLC indicated
37 substitution was complete. The reaction was poured into water and extracted 3x with DCM. Combined
38 organic layers were dried over MgSO₄ and concentrated in vacuo. The crude product was further purified
39 by column chromatography (0-100% EtOAc in Hexanes gradient) to afford the desired intermediate **Int-**
40
41
42
43
44
45
46
47
48
49 **2b**.
50
51
52
53

54 55 **General Procedure B2: Cyanation**

1
2
3 A dry pressure vessel was charged with the appropriate triazinyl chloride (1.0 eq), and suspended
4 in DMSO/H₂O 9:1. KCN (1.1 eq) and 1,4-diazabicyclo[2.2.2]octane (DABCO, 2.0 eq) were added and
5 the reaction was heated to 80°C. Reaction was left to stir at this temperature until LC/MS showed
6 completion of the reaction (6-12 h). Reaction was cooled to room temperature, diluted with EtOAc and
7 washed thoroughly with brine (3-5 x). The organic layer was separated, dried over MgSO₄, filtered, and
8 evaporated. The crude product was further purified by column chromatography (0-100% EtOAc in
9 Hexanes gradient) to afford the desired secondary amine **Int-3b**.
10
11
12
13
14
15
16
17
18
19

20 **General Procedure B3: Alkylation with NaH and aryl/alkyl X/Ms/Ts**

21
22 The triazinyl-nitrile (1 eq) was dissolved in DMF and cooled to -10°C (Ice/Brine bath). 60% NaH
23 in mineral oil (1-1.5 eq) was added and reaction was stirred for 30 min. The appropriate alkyl or aryl
24 Br/Cl/Ms/Ts (1-2 eq) was then added. The reaction was allowed to slowly warm to room temperature and
25 left to stir (2-12 hr) until HPLC indicated reaction was complete. The solution was poured into EtOAc,
26 washed 3x with brine, dried over NaSO₄, and concentrated. Crude residue was purified by flash
27 chromatography EtOAc:Hexanes 0-100% gradient to give the pure tertiary amine **Int-4b**.
28
29
30
31
32
33
34
35
36

37 **General Procedure B4: Boc-Deprotection**

38
39 The Boc-protected amine (1 eq) was dissolved into a 1:2 mixture of TFA:DCM (~0.1-0.3 mM)
40 and allowed to stir at room temperature for 0.5-2h, until HPLC or TLC indicated reaction was complete.
41 Solvent was removed in vacuo and compound was purified by reverse phase chromatography (C18, 10-
42 100% ACN in water + 0.1% TFA gradient) and concentrated to afford desired product as the TFA salt.
43
44
45
46
47
48
49

50 **Computational Modeling:** To construct a model for TgCatL-triazine complex, the X-ray structure of
51 TgCPL in complex with its propeptide (PDB: 3F75) was superposed with the X-ray structure of HsCPL
52 (PDB: 5MAJ) using The Molecular Operating Environment (MOE), version 2008.10, Chemical
53 Computing Group Inc., Montreal, Quebec, Canada. Then, the HsCPL enzyme from the 5MAJ and the
54
55
56
57
58
59
60

1
2
3 propeptide of *TgCPL* from the 3F75 were removed and the *TgCPL* enzyme and the triazine compound are
4 saved as a model for *TgCPL*-triazine complex. All the water molecules from the 3F75 and water
5 molecules outside the binding site from 5MAJ were removed. Covalent docking of the triazine compound
6 in the *TgCPL* was performed with induced fit option instead of rigid receptor for refinement. The covalent
7 docking protocol in MOE was developed by creating a reaction profile for this particular virtual reaction
8 and saving in the MarvinSketch 17.14.0 (<http://www.chemaxon.com>).
9
10
11
12
13
14
15
16
17

18 ***TgCPL* and *HsCPL* Inhibition Assay:** Compound potency and selectivity was evaluated *in vitro* for
19 both *TgCPL* and *HsCPL* activity in a fluorescence-based assay by monitoring the hydrolysis of Cbz-Leu-
20 Arg-aminomethylcoumarin (Z-L-R-AMC). Protein was expressed and purified as described previously.²⁵
21 The substrate hydrolysis results in the release of fluorescent 7-amino-4-methylcoumarin (AMC) that can
22 be monitored spectrophotometrically with linear kinetics for up to 60 min. Inhibitors were serial diluted in
23 DMSO in a 1-to-3 dilution, spanning at least 10 concentration points in either duplicate or triplicate. The
24 enzyme was pre-incubated with the inhibitory compounds for 5 min at 23°C, followed by the addition of
25 the AMC substrate. The assay final conditions had a total volume of 200 μ L, consisting of 90 μ L enzyme
26 (conc.=50 ng/mL), 100 μ L Z-L-R-AMC substrate (conc.= 80 μ M), and 10 μ L inhibitor or DMSO. The
27 relative fluorescence of the AMC generation is measured over the course of 5 min (Excitation: 380 nm,
28 Emission: 460 nm). LHVS (**1**) and DMSO were used as positive and negative controls, respectively. All
29 dose response data was obtained with at least three independent replicates (n=3). Graphpad Prism
30 software was used to visualize inhibition curves and calculate IC₅₀ values from the reaction mean v.
31 Assay final concentrations in each well: 40 μ M ZLR-AMC, *TgCPL* or *HsCPL* (final conc= 0.0225
32 ng/ μ L). Assay Buffer: 100 mM NaAc, 2 mM EDTA, 900 mM NaCl, 50 mM DTT. Substrate: Cbz-Leu-
33 Arg-AMC (Bachem, purchased as HCl salt).
34
35
36
37
38
39
40
41
42
43
44
45
46
47
48
49
50
51
52
53

54 **High throughput library screen:** We utilized compound libraries provided by the University of
55 Michigan Center for Chemical Genomics (CCG) to screen for inhibitors against *TgCPL*. The HTS
56
57
58
59
60

1
2
3 primary screen was conducted on ~150,000 candidates, representing a wide diversity of structures and
4 sources. The libraries were composed of small molecule compounds and clinically tested bioactive drugs
5 obtained from a variety of sources include ChemBridge, ChemDiv, Maybridge, MicroSource, TimTec,
6 NCI, and the NIH Clinical Collection. Reactions of the aforementioned Z-Leu-Arg-AMC assay were
7 conducted in a 384-well plate at the scale of 10 μ L per well. Each reaction was initiated by the addition of
8 50 nL of 2 mM stocks of the compounds to each well using a Caliper Sciclone ALH3000 with a V&P
9 pintool, resulting in a final concentration of 10 μ M for each compound. A Thermo Multidrop Combi
10 Liquid Dispenser was used to add 5 μ L of recombinant TgCPL (0.5 μ g/mL) and 5 μ L of Z-Leu-Arg-
11 AMC (80 μ M), both diluted in activity assay buffer. After 10 min incubation at RT, 10 μ L of E64 (100
12 μ M) diluted in assay buffer was added with the multidrop reagent dispenser. A Perkin Elmer Envision
13 Multimode Plate Reader measured the fluorescence after 30 min at RT with excitation at 355 and the
14 emission at 460 nm. Active compounds were triaged using computational and experimental results to
15 eliminate compounds likely to interfere with the assay or to present development issues. Computational
16 evaluation of primary screen hits was first conducted in light of toxicity, cysteine reactivity, promiscuity,
17 and inhibitor level. Primary screen hits available after this attribute triage were then subjected to
18 confirmation screen to compose the experimental evaluation. Assay conditions from the primary screen
19 were repeated, but conducted in triplicate for each candidate (using a TTP Labtech Mosquito X1 for
20 compound addition). Confirmed hits were retested to establish a concentration response curve of activity
21 in a secondary screen. Assay conditions were repeated on the 384-well plates, and conducted in duplicate
22 for each compound. Compounds found active after the concentration response secondary screen were
23 prioritized based on chemical properties, and given appropriate rankings by consulting medicinal
24 chemists. High and medium ranked hits were prioritized, and fresh powders of the library stocks were
25 obtained from Sigma Aldrich. The available compounds were reconstituted in DMSO to 10 μ M. All assay
26 conditions of the concentration response screen were repeated for the repurchased compounds against
27 both TgCPL and HsCPL.
28
29
30
31
32
33
34
35
36
37
38
39
40
41
42
43
44
45
46
47
48
49
50
51
52
53
54
55
56
57
58
59
60

1
2
3
4
5 **Metabolic Stability in Mouse Liver Microsomes:** The metabolic stability was assessed using CD-1
6 mouse liver microsomes. One micromolar of each compound was incubated with 0.5 mg/mL microsomes
7 and 1.7 mM cofactor β -NADPH in 0.1 M phosphate buffer (pH = 7.4) containing 3.3 mM $MgCl_2$ at 37
8 $^{\circ}C$. The DMSO concentration was less than 0.1% in the final incubation system. At 0, 5, 10, 15, 30, 45,
9 and 60 min of incubation, 40 μ L of reaction mixture were taken out, and the reaction is quenched by
10 adding 3-fold excess of cold acetonitrile containing 100 ng/mL of internal standard for quantification. The
11 collected fractions were centrifuged at 15000 rpm for 10 min to collect the supernatant for LC-MS/MS
12 analysis, from which the amount of compound remaining was determined. The natural log of the amount
13 of compound remaining was plotted against time to determine the disappearance rate and the half-life of
14 tested compounds.
15
16
17
18
19
20
21
22
23
24
25
26
27

28 **Pharmacokinetic Studies in Mice:** All animal experiments in this study were approved by the University
29 of Michigan Committee on Use and Care of Animals and Unit for Laboratory Animal Medicine. The
30 abbreviated pharmacokinetics for compounds was determined in female CD-1 mice following
31 intraperitoneal (ip) injection at 10 mg/kg. Compound was dissolved in the vehicle containing 15% (v/v)
32 DMSO, 15-20% (v/v) PEG-400, and 70% (v/v) PBS. Four blood samples (50 μ L) were collected over 7 h
33 (at 0.5h, 2h, 4h, and 7h), centrifuged at 3500 rpm for 10 min, and plasma was frozen at $-80^{\circ}C$ for later
34 analysis. Plasma concentrations of the compounds were determined by the LC-MS/MS method
35 developed and validated for this study. The LC-MS/MS method consisted of a Shimadzu HPLC system,
36 and chromatographic separation of tested compound which was achieved using a Waters Xbridge-C18
37 column (5 cm \times 2.1 mm, 3.5 μ m). An AB Sciex QTrap 4500 mass spectrometer equipped with an
38 electrospray ionization source (ABI-Sciex, Toronto, Canada) in the positive-ion multiple reaction
39 monitoring (MRM) mode was used for detection. All pharmacokinetic parameters were calculated by
40 non-compartmental methods using WinNonlin, version 3.2 (Pharsight Corporation, Mountain View, CA,
41 USA).
42
43
44
45
46
47
48
49
50
51
52
53
54
55
56
57
58
59
60

1
2
3
4
5 **MDR1/MDCK Assay:** 12-well transwell plates were seeded with MDCKII-MDR1 cells (0.5
6 million/well) and cultured for 24h. Cells were washed with DMEM 3 times (both sides). 0.5 ml of 1 μ M
7 test compound in DMEM was added to apical side (for A to B measurement) or basolateral side (for B to
8 A) (donor side) and 0.5ml of DMEM+0.1% DMSO to the receiving side. Cells were incubated for 4h and
9 2 x 200 μ L was sampled from the receiving side and stored at -20 $^{\circ}$ C for future use. For calibration
10 standard, compound standards were dissolved in DMSO then further diluted in acetonitrile to a
11 concentration of 10 μ g/mL. Calibration standards were prepared from this stock with internal standard (5
12 nM CE302). Samples were prepared by protein precipitation from media followed by addition of internal
13 standard. Samples were analyzed by LC–MS/MS. The LC–MS/MS method consisted of a Shimadzu
14 HPLC system, and chromatographic separation of tested compound which was achieved using a Waters
15 Xbridge-C18 column (5 cm \times 2.1 mm, 3.5 μ m). An AB Sciex QTrap 4500 mass spectrometer equipped
16 with an electrospray ionization source (ABI-Sciex, Toronto, Canada) in the positive-ion multiple reaction
17 monitoring (MRM) mode was used for detection.
18
19
20
21
22
23
24
25
26
27
28
29
30
31
32
33

34 **Bradyzoite Viability Assay:** Bradyzoite viability was assessed by combining plaque assay and
35 quantitative polymerase chain reaction (qPCR) analysis of genome number, as previously performed by
36 Di Cristina *et al*, 2017.²⁶ Briefly, human foreskin fibroblast (HFF) cells were infected with *T. gondii*
37 tachyzoites in six-well plates. Following host cell invasion by parasites, tachyzoites underwent
38 differentiation to bradyzoites by being maintained at 37 $^{\circ}$ C/0% CO₂ in alkaline media (RPMI 1540 w/o
39 NaHCO₃, 50 mM HEPES, 3% FBS, Pen/Strep, pH 8.2), resulting in the generation of *in vitro* tissue cysts.
40 Differentiation was carried out over the course of seven days, replacing the alkaline media daily. Samples
41 were subsequently treated with the test compounds for seven days, replacing them daily. A DMSO-treated
42 vehicle control sample was also incorporated into each assay. Following the treatment period, the culture
43 media in each well was replaced with 2 mL HBSS and cysts were liberated from the infected HFF
44 monolayers by mechanical extrusion, by lifting cells with a cell scraper and syringing several times
45
46
47
48
49
50
51
52
53
54
55
56
57
58
59
60

1
2
3 through 26G needles. Then, 2 mL of pre-warmed 2× pepsin solution (0.026% pepsin in 170 mM NaCl
4 and 60 mM HCl, final concentration) was added to each sample and sample were left to incubate at 37 °C
5
6 for 30 min. Reactions were stopped by adding 94 mM Na₂CO₃, removing the supernatant after
7
8 centrifugation at 1,500g for 10 min at room temperature and re-suspending pepsin-treated parasites in 1
9
10 mL of DMEM without serum. Parasites were enumerated and 1000 parasites per well were added to six-
11
12 well plates containing confluent monolayers of HFFs in D10 media, in triplicate. To allow for the
13
14 formation of plaques, parasites were left to grow undisturbed for 12 days. After this period, the number of
15
16 plaques in each well was determined by counting plaques with the use of a light microscope. Five
17
18 hundred microlitres of the initial 1 mL of pepsin-treated parasites was used for genomic DNA
19
20 purification, performed using the DNeasy Blood & Tissue Kit (Qiagen). Genomic DNA was eluted in a
21
22 final volume of 100 µL. To determine the number of parasite genomes per microliter, 10 µL of each
23
24 gDNA sample was analysed by qPCR, in duplicate, using the tubulin primers TUB2.RT.F and
25
26 TUB2.RT.R. Quantitative PCR analyses were performed using Brilliant II SYBR Green QPCR Master
27
28 Mix (Agilent) and a Stratagene Mx3000PQ-PCR machine. The number of plaques that formed per
29
30 genome was then calculated and expressed as a percentage of control (DMSO) treated parasites.
31
32
33
34
35

36 **HFF Cell Viability by MTS Assay:** MTS assays were performed to evaluate the cytotoxicity of test
37
38 compounds on HFF cells in vitro. HFF cells were plated onto 96-well plates and allowed to become fully
39
40 confluent at 37°C/5% CO₂, prior to the addition of the test compounds. Test compounds were diluted to
41
42 100 µM in conversion media (the same culture media used in bradyzoite viability assays) and applied to
43
44 HFF cells in triplicate. Subsequently, test compounds underwent two-fold serial dilution across the plate
45
46 to a concentration of 0.195 µM. Plates were incubated for a further 7 days at 37°C/5% CO₂, replacing the
47
48 media daily to apply fresh compounds. Following the 7-day treatment, 20 µl of CellTiter 96 Aqueous One
49
50 Solution reagent (Promega) was added to each well and left to incubate for 2 hours at 37°C. Absorbance
51
52 was then measured at 490nm using a Synergy H1 Hybrid Multi-Mode Reader (BioTek). MTS assays
53
54 were performed in triplicate. Untreated HFF cells were used as a negative control. HFF cell viability was
55
56
57
58
59
60

1
2
3 calculated as a percentage by dividing the measured A_{490} of test samples by the mean A_{490} of the untreated
4 control samples. The 50% toxicity dosage (TD_{50}) of each test compound was established by plotting the
5 % HFF cell viability against compound concentration and reading the concentration at 50% HFF cell
6 viability.
7
8
9
10

11 12 13 **ASSOCIATED CONTENT**

14 15 **Supporting Information**

16 Synthetic procedures for and characterization of all compounds.
17
18
19
20

21 22 **AUTHOR INFORMATION**

23 24 *Corresponding Author:*

25 *E-mail: sdlarsen@med.umich.edu
26
27
28
29
30

31 32 *Author Contributions:*

33 The manuscript was written primarily by J.D.Z., V.B.C., and S.D.L. The high throughput screen
34 was performed by N.H. and S.V.R. in The University of Michigan Center for Chemical
35 Genomics. J.D.Z. and J.R.H. synthesized compounds and performed the biochemical assays.
36 A.J.G. performed biochemical assays. Bradyzoite and HFF viability assays were performed by
37 D.S. The microsomal stability and pharmacokinetics studies were run by L.W. and overseen by
38 B.W and D.Sun in The University of Michigan Pharmacokinetics Core. J.D.Z and P.L.
39 performed the computational modeling. MDR1/MDCK assays were performed by J.X. and
40 overseen by R.F.K. All authors have given approval to the final version of the manuscript.
41
42
43
44
45
46
47
48
49
50
51
52
53

54 55 *Funding Sources:*

56 This work was supported by NIAID of the National Institutes of Health under award number
57
58
59
60

1
2
3 R21/R33AI127492 (V.B.C. and S.D.L.). Its contents are solely the responsibility of the authors and do
4
5 not necessarily represent the official views of the NIH. V.B.C. and S.D.L. were also supported by a grant
6
7 from the Center for Discovery of New Medicines, University of Michigan. J.D.Z. acknowledges support
8
9 from the University of Michigan Pharmacological Sciences Training Program (PSTP) training grant (T32-
10
11 GM007767), and the Rackham Merit Fellowship (RMF).
12
13
14
15

16 ***Notes:***

17
18 The authors declare no competing financial interest.
19
20
21
22
23
24
25
26
27
28
29
30
31
32
33
34
35
36
37
38
39
40
41
42
43
44
45
46
47
48
49
50
51
52
53
54
55
56
57
58
59
60

References

1. Dubey, J. P.; Jones, J. L., Toxoplasma gondii infection in humans and animals in the United States. *Int J Parasitol* **2008**, *38* (11), 1257-78.
2. Jones, J. L.; Kruszon-Moran, D.; Elder, S.; Rivera, H. N.; Press, C.; Montoya, J. G.; McQuillan, G. M., Toxoplasma gondii Infection in the United States, 2011-2014. *Am J Trop Med Hyg* **2018**, *98* (2), 551-557.
3. Hoffmann, S.; Batz, M. B.; Morris, J. G., Jr., Annual cost of illness and quality-adjusted life year losses in the United States due to 14 foodborne pathogens. *J Food Prot* **2012**, *75* (7), 1292-302.
4. Scallan, E.; Griffin, P. M.; Angulo, F. J.; Tauxe, R. V.; Hoekstra, R. M., Foodborne illness acquired in the United States--unspecified agents. *Emerg Infect Dis* **2011**, *17* (1), 16-22.
5. Innes, E. A., A brief history and overview of Toxoplasma gondii. *Zoonoses Public Health* **2010**, *57* (1), 1-7.
6. Dubey, J. P., History of the discovery of the life cycle of Toxoplasma gondii. *Int J Parasitol* **2009**, *39* (8), 877-82.
7. Fuglewicz, A. J.; Piotrowski, P.; Stodolak, A., Relationship between toxoplasmosis and schizophrenia: A review. *Adv Clin Exp Med* **2017**, *26* (6), 1031-1036.
8. Afonso, C.; Paixao, V. B.; Costa, R. M., Chronic Toxoplasma infection modifies the structure and the risk of host behavior. *PLoS One* **2012**, *7* (3), e32489.
9. Nascimento, F. S.; Dantas, C. D.; Netto, M. P.; Mella, L. F. B.; Suzuki, L. A.; Banzato, C. E. M.; Rossi, C. L., Prevalence of antibodies to Toxoplasma gondii in patients with schizophrenia and mood disorders. *Schizophr Res* **2012**, *142* (1-3), 244-245.
10. Pearce, B. D.; Kruszon-Moran, D.; Jones, J. L., The Relationship Between Toxoplasma Gondii Infection and Mood Disorders in the Third National Health and Nutrition Survey. *Biol Psychiat* **2012**, *72* (4), 290-295.
11. Lanjewar, D. N.; Surve, K. V.; Maheshwari, M. B.; Shenoy, B. P.; Hira, S. K., Toxoplasmosis of the central nervous system in the acquired immunodeficiency syndrome. *Indian J Pathol Microbiol* **1998**, *41* (2), 147-51.
12. Dediccoat, M.; Livesley, N., Management of toxoplasmic encephalitis in HIV-infected adults--a review. *S Afr Med J* **2008**, *98* (1), 31-2.
13. Deng, Y.; Wu, T.; Zhai, S. Q.; Li, C. H., Recent progress on anti-Toxoplasma drugs discovery: Design, synthesis and screening. *Eur J Med Chem* **2019**, *183*, 111711.
14. Rutaganira, F. U.; Barks, J.; Dhason, M. S.; Wang, Q.; Lopez, M. S.; Long, S.; Radke, J. B.; Jones, N. G.; Maddirala, A. R.; Janetka, J. W.; El Bakkouri, M.; Hui, R.; Shokat, K. M.; Sibley, L. D., Inhibition of Calcium Dependent Protein Kinase 1 (CDPK1) by Pyrazolopyrimidine Analogs Decreases Establishment and Reoccurrence of Central Nervous System Disease by Toxoplasma gondii. *J Med Chem* **2017**, *60* (24), 9976-9989.
15. Sajid, M.; McKerrow, J. H., Cysteine proteases of parasitic organisms. *Mol Biochem Parasitol* **2002**, *120* (1), 1-21.
16. Ang, K. K. H.; Ratnam, J.; Gut, J.; Legac, J.; Hansell, E.; Mackey, Z. B.; Skrzypczynska, K. M.; Debnath, A.; Engel, J. C.; Rosenthal, P. J.; McKerrow, J. H.; Arkin, M. R.; Renslo, A. R., Mining a Cathepsin Inhibitor Library for New Antiparasitic Drug Leads. *Plos Neglect Trop D* **2011**, *5* (5).
17. Sajid, M.; McKerrow, J. H., Cysteine proteases of parasitic organisms (vol 120, pg 1, 2002). *Mol Biochem Parasit* **2002**, *121* (1), 159-159.
18. Chung, J. Y.; Bae, Y. A.; Na, B. K.; Kong, Y., Cysteine protease inhibitors as potential antiparasitic agents. *Expert Opin Ther Pat* **2005**, *15* (8), 995-1007.
19. Dou, Z.; Carruthers, V. B., Cathepsin proteases in Toxoplasma gondii. *Adv Exp Med Biol* **2011**, *712*, 49-61.

- 1
2
3 20. Dou, Z.; Coppens, I.; Carruthers, V. B., Non-canonical maturation of two papain-family proteases
4 in *Toxoplasma gondii*. *J Biol Chem* **2013**, *288* (5), 3523-34.
- 5 21. Dou, Z.; McGovern, O. L.; Di Cristina, M.; Carruthers, V. B., *Toxoplasma gondii* ingests and digests
6 host cytosolic proteins. *MBio* **2014**, *5* (4), e01188-14.
- 7 22. Huang, R.; Que, X. C.; Hirata, K.; Brinen, L. S.; Lee, J. H.; Hansell, E.; Engel, J.; Sajid, M.; Reed, S.,
8 The cathepsin L of *Toxoplasma gondii* (TgCPL) and its endogenous macromolecular inhibitor, toxostatin.
9 *Mol Biochem Parasit* **2009**, *164* (1), 86-94.
- 10 23. Parussini, F.; Coppens, I.; Shah, P. P.; Diamond, S. L.; Carruthers, V. B., Cathepsin L occupies a
11 vacuolar compartment and is a protein maturase within the endo/exocytic system of *Toxoplasma gondii*.
12 *Mol Microbiol* **2010**, *76* (6), 1340-1357.
- 13 24. Pittman, K. J.; Aliota, M. T.; Knoll, L. J., Dual transcriptional profiling of mice and *Toxoplasma*
14 *gondii* during acute and chronic infection. *BMC Genomics* **2014**, *15*, 806.
- 15 25. Larson, E. T.; Parussini, F.; Huynh, M. H.; Giebel, J. D.; Kelley, A. M.; Zhang, L.; Bogyo, M.; Merritt,
16 E. A.; Carruthers, V. B., *Toxoplasma gondii* Cathepsin L Is the Primary Target of the Invasion-inhibitory
17 Compound Morpholinurea-leucyl-homophenyl-vinyl Sulfone Phenyl. *Journal of Biological Chemistry*
18 **2009**, *284* (39), 26839-26850.
- 19 26. Di Cristina, M.; Dou, Z.; Lunghi, M.; Kannan, G.; Huynh, M. H.; McGovern, O. L.; Schultz, T. L.;
20 Schultz, A. J.; Miller, A. J.; Hayes, B. M.; van der Linden, W.; Emiliani, C.; Bogyo, M.; Besteiro, S.; Coppens,
21 I.; Carruthers, V. B., *Toxoplasma* depends on lysosomal consumption of autophagosomes for persistent
22 infection. *Nat Microbiol* **2017**, *2*, 17096.
- 23 27. Barclay, J.; Clark, A. K.; Ganju, P.; Gentry, C.; Patel, S.; Wotherspoon, G.; Buxton, F.; Song, C.;
24 Ullah, J.; Winter, J.; Fox, A.; Bevan, S.; Malcangio, M., Role of the cysteine protease cathepsin S in
25 neuropathic hyperalgesia. *Pain* **2007**, *130* (3), 225-34.
- 26 28. Zwicker, J. D.; Diaz, N. A.; Guerra, A. J.; Kirchhoff, P. D.; Wen, B.; Sun, D.; Carruthers, V. B.;
27 Larsen, S. D., Optimization of dipeptidic inhibitors of cathepsin L for improved *Toxoplasma gondii*
28 selectivity and CNS permeability. *Bioorg Med Chem Lett* **2018**, *28* (10), 1972-1980.
- 29 29. Di, L.; Rong, H.; Feng, B., Demystifying brain penetration in central nervous system drug
30 discovery. Miniperspective. *J Med Chem* **2013**, *56* (1), 2-12.
- 31 30. Li, Y. Y.; Fang, J.; Ao, G. Z., Cathepsin B and L inhibitors: a patent review (2010 - present). *Expert*
32 *Opin Ther Pat* **2017**, *27* (6), 643-656.
- 33 31. Giroud, M.; Ivkovic, J.; Martignoni, M.; Fleuti, M.; Trapp, N.; Haap, W.; Kuglstatler, A.; Benz, J.;
34 Kuhn, B.; Schirmeister, T.; Diederich, F., Inhibition of the Cysteine Protease Human Cathepsin L by
35 Triazine Nitriles: AmideHeteroarene pi-Stacking Interactions and Chalcogen Bonding in the S3 Pocket.
36 *ChemMedChem* **2017**, *12* (3), 257-270.
- 37 32. Ehmke, V.; Winkler, E.; Banner, D. W.; Haap, W.; Schweizer, B.; Rottmann, M.; Kaiser, M.;
38 Freymond, C.; Schirmeister, T.; Diederich, F., Optimization of Triazine Nitriles as Rhodesain Inhibitors:
39 StructureActivity Relationships, Bioisosteric Imidazopyridine Nitriles, and X-ray Crystal Structure Analysis
40 with Human CathepsinL. *Chemmedchem* **2013**, *8* (6), 967-975.
- 41 33. Giroud, M.; Harder, M.; Kuhn, B.; Haap, W.; Trapp, N.; Schweizer, W. B.; Schirmeister, T.;
42 Diederich, F., Fluorine Scan of Inhibitors of the Cysteine Protease Human Cathepsin L: Dipolar and
43 Quadrupolar Effects in the pi-Stacking of Fluorinated Phenyl Rings on Peptide Amide Bonds.
44 *Chemmedchem* **2016**, *11* (10), 1042-1047.
- 45 34. Cai, J.; Fradera, X.; van Zeeland, M.; Dempster, M.; Cameron, K. S.; Bennett, D. J.; Robinson, J.;
46 Popplestone, L.; Baugh, M.; Westwood, P.; Bruin, J.; Hamilton, W.; Kinghorn, E.; Long, C.; Uitdehaag, J.
47 C., 4-(3-Trifluoromethylphenyl)-pyrimidine-2-carbonitrile as cathepsin S inhibitors: N3, not N1 is critically
48 important. *Bioorg Med Chem Lett* **2010**, *20* (15), 4507-10.
- 49 35. Cai, J.; Bennett, D. J.; Rankovic, Z.; Dempster, M.; Fradera, X.; Gillespie, J.; Cumming, I.; Finlay,
50 W.; Baugh, M.; Boucharens, S.; Bruin, J.; Cameron, K. S.; Hamilton, W.; Kerr, J.; Kinghorn, E.; McGarry, G.;

- 1
2
3 Robinson, J.; Scullion, P.; Uitdehaag, J. C.; van Zeeland, M.; Potin, D.; Saniere, L.; Fouquet, A.; Chevallier,
4 F.; Deronzier, H.; Dorleans, C.; Nicolai, E., 2-Phenyl-9H-purine-6-carbonitrile derivatives as selective
5 cathepsin S inhibitors. *Bioorg Med Chem Lett* **2010**, *20* (15), 4447-50.
- 6 36. Altmann, E.; Cowan-Jacob, S. W.; Missbach, M., Novel purine nitrile derived inhibitors of the
7 cysteine protease cathepsin K. *J Med Chem* **2004**, *47* (24), 5833-6.
- 8 37. Schroder, J.; Noack, S.; Marhofer, R. J.; Mottram, J. C.; Coombs, G. H.; Selzer, P. M., Identification
9 of semicarbazones, thiosemicarbazones and triazine nitriles as inhibitors of *Leishmania mexicana*
10 cysteine protease CPB. *PLoS One* **2013**, *8* (10), e77460.
- 11 38. Turk, V.; Stoka, V.; Vasiljeva, O.; Renko, M.; Sun, T.; Turk, B.; Turk, D., Cysteine cathepsins: from
12 structure, function and regulation to new frontiers. *Biochim Biophys Acta* **2012**, *1824* (1), 68-88.
- 13 39. Gauthier, J. Y.; Chauret, N.; Cromlish, W.; Desmarais, S.; Duong, L. T.; Falguyret, J. P.; Kimmel,
14 D. B.; Lamontagne, S.; Leger, S.; LeRiche, T.; Li, C. S.; Masse, F.; McKay, D. J.; Nicoll-Griffith, D. A.; Oballa,
15 R. M.; Palmer, J. T.; Percival, M. D.; Riendeau, D.; Robichaud, J.; Rodan, G. A.; Rodan, S. B.; Seto, C.;
16 Therien, M.; Truong, V. L.; Venuti, M. C.; Wesolowski, G.; Young, R. N.; Zamboni, R.; Black, W. C., The
17 discovery of odanacatib (MK-0822), a selective inhibitor of cathepsin K. *Bioorg Med Chem Lett* **2008**, *18*
18 (3), 923-8.
- 19 40. Talele, T. T., The "Cyclopropyl Fragment" is a Versatile Player that Frequently Appears in
20 Preclinical/Clinical Drug Molecules. *J Med Chem* **2016**, *59* (19), 8712-8756.
- 21
22
23
24
25
26
27
28
29
30
31
32
33
34
35
36
37
38
39
40
41
42
43
44
45
46
47
48
49
50
51
52
53
54
55
56
57
58
59
60